Petrology and geochemistry of the Texenna ophiolites, northeastern Algeria: Implications for the Maghrebian flysch suture zone

El Hachemi Boukaoud, Gaston Godard, Moulley Charaf Chabou, Youcef Bouftouha, Sidali Doukkari

Petrology and geochemistry of the Texenna ophiolites, northeastern Algeria: Implications for the Maghrebian flysch suture zone

El Hachemi Boukaoud [a, b], Gaston Godard [c, *], Moulley Charaf Chabou [d], Youcef Bouftouha [a], SidAli Doukkari [e, f].

[a] Laboratoire de Génie Géologique, Université Mohamed Seddik Benyahia - Jijel, BP 98 Ouled Aissa, 18000 Jijel, Algeria.

[b] Laboratoire Géologie et Environnement, Université Frères Mentouri Constantine1, Algeria.

[c] Université de Paris, Institut de physique du globe de Paris, CNRS, F-75005 Paris, France.

[d] Emerging Materials Research Unit and Institute of Architecture and Earth Sciences, Department of Earth Sciences, Ferhat Abbas University, Setif 1, Algeria.

[e] Laboratoire de Géodynamique, Géologie de l'Ingénieur et de Planétologie, FSTGAT-U.S.T.H.B., B.P. 32, El Alia, Dar el Beida, 16111-Alger, Algeria.

[f] Département S.N.V, Faculté des Sciences, Université Alger 1, 2 rue Didouche Mourad, Alger, Algeria.

[*]Corresponding author: godard@ipgp.fr

Abstract

This study presents the first geochemical, mineralogical and petrological data on the mafic and ultramafic rocks of Texenna (Lesser Kabylia, north-eastern Algeria) with the aim of constraining their tectonic setting in the context of the Maghrebide belt. The magmatic-sedimentary complex of Texenna comprises serpentinite, metabasites (metagabbro, metadolerite and metabasalt with pillow-lava structures), and oceanic metasediments (radiolarite and calcschists). Serpentinites consist mainly of mesh textures and large bastites of lizardite, Cr-spinels altered to "ferritchromit" and chlorite, with chrysotile and chlorite veins. Their features are very similar to those of serpentinites collected from the seafloor. Pillow-lava metabasalts contain mineral assemblages of albite, epidote, chlorite, actinolite and titanite, and, despite metamorphism, have preserved many of the pillow-lava microstructures (former glassy, variolitic and spherulitic zones; former devitrification spherulites and gas vesicles; pseudomorphs after phenocrysts and microliths). Metadolerites and metagabbros have sometimes preserved their magmatic plagioclase, but are generally transformed into an assemblage of albite, calcic amphiboles, chlorite, epidote and titanite, a mineral assemblage typical of the static greenschist-facies hydrothermal metamorphism of an oceanic crust. Some deformation in the conditions of phengite-bearing greenschist-facies metamorphism is linked to the tectonic emplacement of the ophiolites in their current setting during the Maghrebide orogeny.

Geochemically, the whole-rock compositions of the serpentinites indicate a harzburgite protolith, while the metabasites are tholeiitic and show the N-MORB signature for the pillow lavas and T-MORB to E-MORB affinities for the intrusive rocks (metadolerites and metagabbros). These results demonstrate for the first time that the magmatic-sedimentary complex of Texenna belongs to a true ophiolitic slice and indicate that the sedimentary cover of the Maghrebian Flysch domain was deposited over a true oceanic rather than a thinned continental crust. The Texenna ophiolites show analogies with many other ophiolites in the Western Mediterranean region, indicating that they represent remnants of the ancient oceanic lithosphere of the western Tethys (*i.e.*, Maghrebian Tethys Ocean) that formed between Africa and Iberia during the Middle-Late Jurassic.

Keywords: Ophiolites, Maghrebian Flysch, Texenna, Maghrebide belt, Algeria, Western Tethys.

Introduction

Ophiolites are geological markers of prime importance for understanding the geodynamic evolution of orogenic belts (*e.g.*, Furnes and Safonova, 2019). They often occur in suture zones that mark the closure sites of the ancient oceanic domain. In the southern part of the circum-Mediterranean Alpine belt, the Maghrebide chain would be such a suture zone, resulting from the Cenozoic collision of fragments of the AlKaPeCa microcontinent (*i.e.*, Alboran, Kabyle, Peloritan and Calabrian blocks) with Africa, respectively at the origin of the internal (*i.e.*, northern) and external (southern) zones of the chain (Durand-Delga and Fontobé, 1980; Bouillin, 1986). The suture zone is underlined by allochthonous flysch deposits (Frizon de Lamotte et al., 2011), with slices of mafic rocks with ophiolite affinities (Fig. 1), well known in the Rif (Morocco) and Sicily (*e.g.*, Durand-Delga et al., 2000). Similar mafic rocks have been reported at the base of the Maghrebian flysch, in various localities of northern Algeria, both in Greater Kabylia (Chellata massif) and Lesser Kabylia (Texenna, Moul Ed-Demamene massif, Fedj el Mekta') (Durand-Delga, 1948, 1949, 1950, 1954, 1955; Coutelle and Gélard, 1968; Bouillin, 1974, 1986; Bouillin and Hernandez, 1975; Bouillin et al., 1977). In the Texenna region, in particular, an association of mafic and ultramafic rocks occurs beneath the Maghrebian flysch nappes at the southern front of the internal zones of Lesser Kabylia (Durand-Delga, 1949, 1950, 1955; Bouillin et al., 1977). The occurrence near Texenna of serpentinites, metagabbros, pillow lavas and radiolarites likely represents the only complete ophiolite suite of the Maghrebian flysch suture zone (Bouillin, 1986). However, the last studies carried out on this formation date back to the 1970s (*e.g.*, Durand-Delga, 1971; Bouillin et al., 1977), so that new investigations are necessary to better characterize the only ophiolite suite known to date in the Algerian part of the Maghrebide chain.

Major and trace element geochemistry of ophiolitic mafic rocks provides important clues for unravelling the tectonic setting of ophiolites. Furthermore, immobile element geochemistry is an important tool for investigating ophiolitic rocks, since ophiolites experience intense alteration and metamorphism before, during and after being involved in orogenic processes (*e.g.*, Pearce, 2014). Very little geochemical data are available for the mafic rocks associated with the Maghrebian flysch zone. Durand-Delga et al. (2000) presented a few geochemical analyses of Jurassic basic rocks associated with the Maghrebian flyschs of the Rif (Morocco) and Sicily (Italy), indicating their E-MORB affinity. Roman'ko et al. (1998) gave geochemical composition of basalt from Moul Ed-Demamene massif (Lesser Kabylia, Algeria). However, no geochemical analysis has been published for the mafic and ultramafic rocks of the Texenna region. In addition, although petrographic descriptions of the Texenna rocks have already been made using a polarizing optical microscope (Durand-Delga, 1955, 1971; Bouillin et al., 1977), a detailed petrological study remains necessary to decipher the formation of these magmatic rocks and their metamorphic evolution.

The purpose of this paper is to present the first mineralogical, petrological and geochemical data on the mafic and ultramafic rocks of Texenna and to discuss their geodynamic implications in the context of the Maghrebide chain.

Regional geology

Maghrebide chain

The Maghrebide chain, which extends in northern Morocco and Algeria (Fig. 1), includes three main parallel tectonic domains, from north to south (for a recent review, see Leprêtre et al., 2018): (i) the internal zones, belonging to the AlKaPeCa microcontinent; (ii) the Maghrebian flysch nappes, consisting of remnants of the Ligurian-Maghrebian Tethys oceanic basin; and (iii) the external zones, interpreted as the North-African palaeomargin inverted during the Cenozoic collision. The ophiolitic rocks studied here are in the vicinity of the Maghrebian flysch units, which, depending upon their position within the initial basin, are traditionally divided into two main stratigraphic sequences (Bouillin et al., 1970): the Mauretanian series, originally close to the southern margin of the AlKaPeCa microcontinent and the Massylian series, near the African palaeomargin.

Internal zones

In the study area (Fig. 2a), the internal zones consist of two metamorphic groups (Bouillin et al., 1977): a retro-metamorphosed lower group composed of gneiss and white-micaschist, and an upper

group with granulite-facies rocks, including garnet-kyanite “leptynites” (*i.e.*, leucocratic gneiss), garnet pyroxenites, metagabbros and forsterite marbles.

In various places near Texenna, the Kabyle basement contains intercalations of pyroxenite, amphibolite and layered metagabbro, from a few centimetres to a metre in thickness (Bouillin et al., 1977; Djellit, 1987). Their mineralogical assemblages, essentially anhydrous, are dominated by pyroxenes with oriented granoblastic texture, and were formed under granulite- and/or amphibolite-facies metamorphic conditions. A layered metagabbro, dated by the U-Pb method on titanite, provided ages at 315 and 239 Ma (unpublished data), and seems therefore linked to the Hercynian orogeny. Peridotite meter-thick levels, with olivine + Cpx + Opx ± plagioclase ± spinel, were also observed along the thrust that separates the Kabyle basement from the Texenna ophiolites (Fig. 2). Subject to a petrological and geochemical study in progress, these peridotites also seem to be linked to the Kabyle basement. These mafic and ultramafic rocks of the basement contrast with those of the Texenna ophiolites by their high-grade anhydrous metamorphism and their probable Hercynian age, and are therefore not considered in this study.

The Kabyle metamorphic basement is overlain by the so-called “Dorsale calcaire” (Raoult, 1974), which consists of unmetamorphosed sediments, of either Palaeozoic (Baudelot et al., 1981) or Upper Jurassic to Lutetian age, interpreted as deposited along the passive margin between the AlKaPeCa continent and the Ligurian Tethys by several authors (*e.g.*, Bouillin, 1992). Two kilometres northeast of the gorge of Oued Djendjene, Silurian graptolitic shales lie unconformably on the Kabyle basement (Durand-Delga, 1955), which is also unconformably overlain by the much more recent clastic deposits of the Oligo-Miocene Kabyle unit (Djebel el Kelaa; Fig. 2a) dated from Late Oligocene to Burdigalian (Bouillin, 1979).

Flysch domain

Cretaceous turbidite sequences (“flyschs”) are widespread in the region of Texenna, where they form the Massylian and Mauritanian units. According to Bouillin et al. (1977), the Mauritanian flysch of Djebel Es-Sendouah is in continuity with the Texenna green rocks and the overlying radiolarites and carbonate rocks. It is composed of interbedded thick layers of slightly metamorphosed lustrous pelitic schists and quartzitic sandstones. Some unmetamorphosed Mauritanian flysch (“Flysch de Guerrouch”) outcrops in the western and northern part of the study area (Fig. 2a). Further south, some Albian-Aptian flysch in 10-cm thick layers, of Massylian affinity, are overlain by Albian-Cenomanian shales with microbreccias and black phtanites. A tectonic contact separates the Mauritanian flysch of Djebel Es-Sendouah (Mauritanian flyschs) from the Massylian flysch (Bouillin et al., 1977).

The occurrence in the region of Texenna of large undeformed and unmetamorphosed klippes of Mauritanian flysch ("Flysch de Guerrouch") over the Kabyle basement and its Oligo-Miocene cover, have led Andrieux and Djellit (1989) and Andrieux et al. (1989) to suggest an internal origin of the "Flysch de Guerrouch", from basins located north of the Kabyle domain ("ultra" flysch). However, this hypothesis has been challenged, spurring intense debates during the 1970s-1980s (*e.g.*, Coutelle and Delteil, 1989; Bouillin, 1989).

External Zones

The Tellian units belong to the external zones and are exposed to the south of the Flysch domain; in the studied area, they correspond to the mid-Tellian units of Wildi (1983). The sedimentary sequence, which ranges in age from Triassic to Lutetian (Paleogene) (Bouillin, 1979), includes Triassic sandstones, Jurassic carbonate rocks, conglomerates and microbreccias of the Upper Cretaceous, and finally black marls with yellowish "balls" of the Upper Cretaceous, Palaeocene and Eocene (Bouillin, 1979). Finally, the region is characterized by large exposures of the Triassic complex composed of red clays, evaporites and mafic vein rocks ("ophites": Durand-Delga, 1955).

Ophiolitic complex of Texenna

Ehrmann (1946) was the first to report on the Tamesguida geological map at 1/50 000 the occurrences of mafic and ultramafic rocks in the region of Texenna. Durand-Delga (1949, 1950, 1955) included these rocks in the Precambrian basement of Lesser Kabylia. Later, by re-examining in detail the outcrops of Texenna, he recognized the possible ophiolitic nature of the mafic-ultramafic complex, affected by a low-grade metamorphism, which he referred to as "Sendouah-Tabellout unit" and placed at the base of the Cretaceous Massylian flysch (Durand-Delga, 1971). Bouillin et al. (1977) reinvestigated the magmatic complex of Texenna and the overlying series, and concluded that the magmatic complex of Texenna could be considered as the upper part of an ophiolitic series.

The magmatic-sedimentary complex of Texenna crops out discontinuously over an area of approximately 21 km^2 (14 km × 1.5 km). It extends from the Es-Sendouah massif in the northwest to Dra-El-Fertasa in the southeast, through the village of Texenna, following the tectonic contact line between the Kabyle basement and the Flysch domain (Fig. 2a, b). At the top of the Es-Sendouah massif, brecciated serpentinites are crosscut by metadolerite veins (Fig. 3a), which in turn form sill-like bodies, a few cm to several m thick, interspersed between calcschist and radiolarite layers near the village of Texenna. Further SSE, Bouillin et al. (1977) and Djellit (1987) subdivided the volcano-sedimentary complex of Texenna into two units: (1) The lower unit is composed of layered igneous rocks showing variable textures (aphyric, porphyritic and coarse-grained); this unit begins with

pillow-lavas associated with recrystallized radiolarites, followed by igneous beds of metabasalts, metadolerites and metagabbros with calcschist intercalations. (2) The upper unit consists of quartzo-pelitic layers, pillow-lavas and dolerites; these rocks are overlain by an alternation of limestone and lustrous calcschist layers, 1 cm to 10 cm thick. These two units, totalling 500 m in thickness, are well exposed in the Tabellout massif, at Djebel Dra-El-Fertasa and in the gorge of Oued Djendjene (Fig. 3e-h).

The magmatic complex of Texenna is overlain by carbonate rocks and radiolarites of presumed Upper Jurassic-Berriasian age, in turn overlapped by Cretaceous pelites and quartzites of the Mauretanian flysch (Bouillin et al., 1977; Bouillin, 1979). All these formations, which are overthrust by the high-grade basement of the internal zones of Lesser Kabylia, are overturned. They are all schistosed and metamorphosed, in particular the magmatic rocks of the Texenna complex which have undergone a greenschist-facies metamorphism (Bouillin et al., 1977).

Material and methods

About 100 samples were collected along a NW-SE profile from Djebel Es-Sendouah to the gorge of the Djendjene valley (Fig. 2a). Many outcrops located in the Djendjene valley to the southwest of the Tabellout dam are now under water, but were surveyed before the impoundment; on the other hand, the dam worksite has revealed new outcrops. Eighteen samples were selected for detailed mineralogical and geochemical analyses (see details on the techniques in Sections 2 and 3 of the Supplementary materials [SM]). The investigated rocks comprise ultramafic rocks (serpentinite), metabasites (metagabbro, metadolerite and metabasalt with some pillow-lava structures), and metasediments (radiolarite and calcschists). Thin sections were investigated under the SEM and at the electron microprobe. Representative microprobe analyses of the various minerals are reported in Tables A–F in SM. Serpentinite samples were also characterized by X-Ray powder diffraction (XRPD: Fig. A in SM). Fifteen samples were selected for whole-rock analyses of major, trace and rare earth elements (REE), using the ICP-AES and ICP-MS methods (see Section 3 and Table G in SM). In order to unravel the *P-T* conditions during the tectonic emplacement, the thermodynamic modelling of a *P-T* pseudosection was carried out for a foliated metabasite, using the Thermocalc software with an upgraded version of the thermodynamic dataset of Holland and Powell (2011) (Section 5 in SM).

Results

Field occurrence, petrology and mineral chemistry

Serpentinites

Small outcrops of serpentinite are scattered in the Sendouah-Tabellout unit. The main outcrop is located in the northeast, at Es-Sendouah crest, and is associated with metadolerites. The serpentinites extend over 700 m in length for a maximum width of 50 m; they are generally compact, sometimes brecciated, dark green to green-black in colour, contain whitish veins of chrysotile and are crosscut by metadolerite dykes, 10 to 20 cm thick (Fig. 3a-b). Several serpentinite lenses are also visible on the southern slope of the Tabellout Massif, about 3 km to the SSE of Texenna (Fig. 2a; *e.g.*, 36°38'27.9"N–5°48'6.3"E; 36°38’17.9"N–5°48'15.9"E). Durand-Delga (1955, pp. 80-83) reported a few other occurrences that are no more visible, mostly along the SW tectonic contact with the Cretaceous flysch: at ca. 36°38’52”N–5°47’34”E; 36°37'31.6"N–5°48'46.3"E (a 200-m long level on the southern bank of Oued Djendjene); 36°37'11.3"N–5°49'21.8"E (a meter-thick lens along the contact with the flysch); and in the vicinity of 36°35'29”N–5°53'26”E.

Under the optical microscope and the scanning electron microscope (SEM), these rocks generally show mesh textures resulting from the serpentinization of olivine grains, large “bastites” formed at the expense of pyroxene, pseudomorphs after Cr-rich spinel and small veins of chrysotile scattered in the rock (Fig. 4).

The mesh texture consists of cells about 0.5 mm in diameter, with a discontinuous edge rich in tiny crystals of magnetite enveloping one or more concentric layers of serpentine towards the nucleus, where no relict olivine has been observed (Fig. 4b). The serpentine is here almost Al- and Ca-free and of fairly homogeneous composition (Table A in SM), despite changes in the intensity of the backscattered electrons (BSE) (Fig. 4b), which seem to be linked to slight variations in the H_2O and Fe contents (rim vs. core in Table A). When calculated on the basis of 3 cations, in order to be compared with $Si_1(Mg, Fe)_2O_4$ of the former olivine, the serpentine composition is on average $Si_{1.337\pm0.069}$ $Al_{0.047\pm0.018}$ $Cr_{0.001\pm0.000}$ $Mg_{1.484\pm0.083}$ $Fe_{0.118\pm0.007}$ $Mn_{0.002\pm0.000}$ $Ca_{0.007\pm0.002}$ $Na_{0.002\pm0.002}$ $K_{0.002\pm0.001}$ (sample Serp2); the higher values of Si and Mg (X_{Mg} = Mg/[Mg+Fe+Mn] = 0.926±0.005) compared to a common olivine can be explained by the concomitant crystallisation of magnetite, which contains only traces of Si and Mg ($Si_{0.008}$ $Ti_{0.000}$ $Cr_{0.001}$ $Fe^{3+}_{1.986}$ $Fe^{2+}_{0.992}$ $Mn_{0.002}$ $Mg_{0.008}$ O_4). *XRPD* analyses of serpentinite shows that serpentine is predominantly lizardite (Fig. A in SM).

Bastites are generally 1 to 4 mm in size, but can reach 1 cm according to Durand-Delga (1955). They are mainly made of serpentine, but also contain chlorite and a Ca-rich and Al-poor clinoamphibole (*i.e.*, tremolite: $[Si_{7.54}\ Al_{0.46}]_T$ $[Al_{0.28}\ Ti_{0.05}\ Cr_{0.01}\ Mg_{3.15}\ Fe^{2+}_{1.51}]_C$ $[Mn_{0.04}\ Ca_{1.90}\ Na_{0.06}]_B$ $[Na_{0.06}\ K_{0.02}]_A$ O_{22} $[OH_{1.99}\ F_{0.01}]$), arranged in parallel grooves (dashed line *in* Fig. 4c). The overall composition of bastite,

obtained by scanning during analysis (see 2 in SM) and calculated on the basis of 4 cations ($Si_{1.714}$ $Al_{0.188}$ $Cr_{0.019}$ $Ti_{0.002}$ $Mg_{1.757}$ $Fe_{0.137}$ $Mn_{0.001}$ $Ca_{0.177}$ $Na_{0.004}$ $K_{0.002}$), can be compared with some Al-rich Ca-bearing orthopyroxene (ideally, Si_{2-x} $[Al, Cr]_{2x}$ $[Mg, Fe]_{2-x-y}$ Ca_y O_6), stable at elevated temperatures. The Ca-rich tremolite-bearing grooves are probably derived from clinopyroxene lamellae exsolved during the cooling of such a high-*T* orthopyroxene protocrystal.

Former spinel crystals have been altered into the so-called "ferritchromit" and are surrounded by a chlorite corona (Fig. 4d). Tiny areas in these "ferritchromit" pseudomorphs are rich in Cr-magnetite (shown in white *in* Fig. 4d), which, being mixed with its matrix, only gave imprecise microprobe analyses ("Cr-magnetite" in Fig. 5e). Other inclusions are made of Al-rich and Si-poor chlorite (corundophyllite in Fig. 5f). Such a "ferritchromit" would in fact consist of a complex cryptocrystalline association of Cr-magnetite, chlorite and lizardite (Mellini et al., 2005). The overall composition of one of these "ferritchromit" grains (Fig. 5b; "bulk" in Table B of SM), obtained by scanning at the microprobe, corresponds quite exactly to a combination of Cr-magnetite (70 mol% of theoretical $Cr_{0.81}Fe^{3+}_{1.19}Fe^{2+}_{1.00}O_4$), chlorite (22 mol%) and serpentine (8 mol%), the relative amounts of which can vary, thus explaining the concentric chemical variations of the pseudomorph (Fig. 4d). The Mg-rich chlorite coronae around the former spinel grains present, from the matrix inwards, a progressive zoning with a not surprising decrease in Si (from 6.87 to 6.00 atoms per formula unit [apfu]) and increases in Al (from 2.69 to 4.15 apfu) and Cr (0.08 to 0.15 apfu), ranging from penninite to clinochlore end-members (triangles *in* Fig. 5f; Table D in SM), according to Hey's (1954) nomenclature; some chlorite included in the former spinel even reaches the composition of a corundophyllite, particularly poor in Si and rich in Al (Fig. 5f). This microstructure can be explained by chemical gradients and exchanges between the former Cr-rich spinel and its serpentine-rich matrix, Al being released from the spinel to form chlorite, while some Si and H_2O from the matrix contributed to the spinel replacement.

Finally, numerous veinlets filled with serpentine (likely chrysotile), tremolite and/or chlorite (close to the former spinel), crosscut the former microstructures (Fig. 4a, d).

The normative mineralogy of the peridotite protolith could be estimated by the least-square method, using the bulk-rock chemical analyses of the serpentinite samples (Table G in SM). The result yields an Opx-rich peridotite, with (in mol%) 53.2 ± 8.8 [1 σ] olivine, 40.1 ± 3.9 Opx, 2.4 ± 2.9 Cpx and 4.3 ± 2.2 spinel, which projects into the harzburgite field of Le Bas and Streckeisen (1991) (Fig. 6). Although this normative mineralogy only gives an approximate picture of the protolith, the composition of which could have been modified during serpentinization, it clearly indicates that the original peridotite was a spinel harzburgite, which is corroborated by the low Ca content of the rocks and the

abundance of bastite pseudomorphs after Opx. Most of the serpentinite samples described by Durand-Delga (1955) are rich in bastite and also derive from harzburgite.

XRPD spectra of serpentinite samples Serp7, Serp17 and Serp18 (Fig. A in SM) show a predominance of lizardite against antigorite, reflecting an hydrothermal serpentinization at low temperature (<350 °C: Reynard, 2013). This serpentinization frequently preserved microstructures inherited from the harzburgite protolith, like the mesh texture after olivine grains, bastite after Opx enclosing former Cpx exsolution lamellae and pseudomorphs after Cr-rich spinel grains. Commonly, these microstructures are almost intact, being affected only by the formation of veinlets linked to some brittle deformation of the serpentinite (Fig. 4d).

Metadolerites and metagabbros

Metadolerites occur in the form of thin dykes that crosscut the Es-Sendouah serpentinites (Fig. 3a) and sills or dykes intrusive into the calcschists (Fig. 3c). They range from a few meters to several tens of meters in length with a thickness up to a few meters. The metadolerites are green to green-yellow and are penetrated by whitish and greenish veins. They frequently retained the doleritic texture of the protolith, showing mm-sized tabular crystals of plagioclase arranged in a matrix mainly consisting of clinoamphiboles (Fig. 7d-e). Other metabasites have also partially retained their magmatic doleritic texture (*e.g.*, Mb11: Fig. 7a-c), but instead of occurring in the form of sills or dykes, they belong to larger masses of metabasites. These rocks, referred to as metagabbros, are common in Oued Missa and Tabellout massif areas (Fig. 2a).

The metadolerites may have preserved their primary plagioclase crystals (*e.g.*, sample Md4: Fig. 7d-e), the magmatic origin of which is attested by their subhedral tabular forms, their zoning with An-rich cores (Md4: An_{68} to An_{40}, from core to rims; Fig. 5d), as well as their double Carlsbad-albite twins (the Carlsbad-twin planes are visible as longitudinal grooves in Fig. 7d-e). Overgrowths of andesine-oligoclase ($An_{38–17}$: blue areas in Fig. 7e) may have formed at least partially during metamorphism. In most cases, however, the former magmatic plagioclase was completely transformed by "saussuritization" into albite ($An_{0.3–2.5}$) associated with some epidote (sample Mb11; Fig. 7a-c). Epidote, common in the most altered samples, shows a ferric molar fraction ($X_{Fe}^{3+} = Fe^{3+} / [Fe^{3+} + Al + Cr]$), that ranges from 0.15 to 0.32 with an average of $X_{Fe}^{3+} = 0.28$, X_{Fe}^{3+} of 1/3 corresponding to the epidote *s.s.* end-member.

The interstices between the former plagioclase laths are mostly filled with amphibole in the less metamorphosed samples (*e.g.*, Md4; Fig. 7e), or with amphibole, chlorite and titanite in the more altered ones (*e.g.*, Mb11; Fig. 7b-c). In the most preserved metadolerites, calcic amphiboles, which replaced the former clinopyroxene of the protolith, show a trend of composition varying between

actinolite, magnesiohornblende, up to ferro-pargasite and Ti-rich pargasite (Fig. 5a-c), preferentially located in the vicinity of plagioclase, which would have facilitated the pargasitic substitution ($Na_{+1}Al^{IV}_{+1}Si_{-1}$) by providing Al and Na. On the other hand, actinolite dominates in the most altered samples, where it replaces magnesio-hornblende on the crystal edges (Fig. 7c). Chlorite is predominantly pycnochlorite (Fig. 5f). The accessory minerals are chlorapatite, fluorapatite, ilmenorutile and ilmenite frequently surrounded by titanite coronae. Veinlets are filled with albite, epidote (Fig. 7a), rarely with potassium feldspar ($Or_{96–97}$), calcite and dolomite.

Although the normative mineralogy of the original gabbros and dolerites may be distorted by changes in rock composition during metamorphism, the calculation of the C.I.P.W. norm, applied to bulk-rock compositions (Table G in SM), reveals that the gabbroic protoliths were close or slightly above the "critical plane of silica undersaturation", with a magmatic paragenesis of Pl + Cpx + Ol ± Opx. The average normative composition is in fact typical of an olivine-tholeiite composition (in wt.%): 58.3 Pl ($An_{51}Ab_{44}Or_5$) + 16.3 Cpx + 14.8 Ol + 2.3 Opx + 2.9 Ilm + 1.5 Mag + 0.3 Ap + 0.1 Chr + 3.5 water.

Pillow lavas

Stacks of pillow lavas are observed in the gorge of the Djendjene valley, near the Tabellout water dam (*e.g.*, 36°36'49.1"N–5°51'00.7"E), where they extend horizontally over 1.2 × 1 km^2 (Fig. 2a), with a thickness from a few to ~25 meters. They are interlayered in places with cm- to m-thick radiolarite and calcschist beds. Because of deformation, the pillows are ellipsoidal (Fig. 3g) and their size varies from a few decimetres to 1.5 metre. They are well recognizable by their concentric structure and the occasional presence of a variolitic zone (Fig. 3h; *e.g.*, 36°36'58.1"N–5°51'11.4"E). Their core is massive, grey and may contain partly-saussuritised plagioclase phenocrysts, whereas the rims are commonly schistose, aphyric and greenish (Fig. 3e).

These metabasalts exhibit a hydrous greenschist-facies metamorphic paragenesis, made of albite, epidote, chlorite, actinolite, titanite and apatite (Fig. 7f-k). They ordinarily do not show relicts of the magmatic assemblage, but instead have commonly preserved microstructures that make it possible to recognize the typical original features of an unmetamorphosed pillow basalt, like the one dredged at the Southwest Indian Ridge and shown in Figure B (in SM):

(i) *Textural zoning*: The detailed study of a section through a pillow shows several concentric zones (Fig. 7f): (a) A thin outer zone with microcrystalline interstitial texture, consisting predominantly of chlorite and minor amounts of epidote and titanite (Z1 in Fig. 7f); (b) variolitic zones, composed of chlorite, actinolite and epidote (Z2 in Fig. 7f), grading into epidote, albite and actinolite (Z3 in Fig. 7f); (c) an inner zone, where epidote with inclusions of albite is dominating (Z4 in Fig. 7f). These zones

probably correspond to the classical concentric zoning that frequently characterizes unaltered pillow lavas, with glassy, variolitic and spherulitic zones (Fig. B in SM).

(ii) *Magmatic flow*: Trails of micro-crystals, especially of titanite, visible in the Z_1 outer zone, close to the surface of the pillow and subparallel to it, could be the vestiges of magmatic flow (1 in Fig. 7g).

(iii) *Phenocrysts*: Polycrystalline clusters of epidote show regular external shapes (2 in Fig. 7g-h), which strongly suggest that they are pseudomorphs after mm-sized phenocrysts of An-rich plagioclase, transformed into epidote during metamorphism. Some porphyritic pillow lavas contain still-preserved zoned plagioclase phenocrysts, ranging in size from a few to ~10 mm. In sample Pil13, these incompletely-saussuritised phenocrysts still show a clear chemical zoning between the apparent centre (An_{23}) and the rims (An_4).

(iv) *Devitrification spherulites*: The greenish varioles visible to the naked eye appear as globular epidote clusters with many albite micro-inclusions under the microscope (3 in Fig. 7g-k). We interpret them as deriving from devitrification spherulites of the basaltic protolith (see, *e.g.*, Arndt and Fowler, 2004), for the following reasons: (a) These globules increase in size and density from the pillow edge (Z1), where they are isolated within chlorite (3 in Fig. 7g), towards the centre of the pillow, where they become contiguous (3 in Fig. 7i) and finally merge (3 in Fig. 7j); this reflects a common feature of the devitrification spherulites, which are progressively less abundant towards the glassy quenched crust (Fig. B). (b) Albite micro-inclusions are often aligned and sheave-shaped inside each epidote globule, similarly to the common fibroradiate microstructure of former spherulites (3 in Fig. 7i). (c) Irregular thin coronae of the same Ep+Ab association almost completely surround some pseudomorphs after plagioclase phenocrysts (3 around 2 in Fig. 7h), which finds a simple explanation by considering that devitrification commonly initiates on the surface of pre-existing plagioclase crystals (Fig. B). (d) Devitrification spherulites in basaltic rocks are essentially made of cryptocrystalline plagioclase, which indeed should evolve into Ep+Ab during low-grade metamorphism.

(v) *Microliths*: In the inner zone of the pillow (Z4), tabular 0.1-mm sized albite microcrystals could derive from former plagioclase microliths (4 in Fig. 7j).

(vi) *Gas vesicles*: Some 0.1-mm spherules behaved like microgeodes, filled with concentric micro-layers of epidote (Pil15: $X_{Fe}^{3+} = Fe^{3+} / [Fe^{3+} + Al + Cr] = 0.326 \pm 0.011$), clinozoisite/epidote (X_{Fe}^{3+} = 0.23–0.13) and chlorite (5 in Fig. 7k). In some samples (*e.g.*, Pil13), eye-shaped vacuoles of several mm are now filled, at the margins, with concentric euhedral growth zones evolving from epidote ($X_{Fe}^{3+} = 0.32$) to clinozoisite ($X_{Fe}^{3+} = 0.11$) and, towards the centre, with chlorite that occupies most of the cavity. All are certainly derived from gas vesicles in the basalt protolith.

In most metabasalts, plagioclase is almost pure albite ($Ab_{98.7\pm1.1}$), but its composition also extends in the oligoclase range, up to An_{28} when plagioclase saussuritization was incomplete (*e.g.*, Pil13; red squares in Fig. 5d). Epidote is close to the epidote *s.s.* end-member (typically, $X_{Fe}^{3+} \approx 0.32$); it is homogeneous in all sites except in the former gas vesicles (see above). Amphibole is most commonly actinolite or magnesio-hornblende (Fig. 5b), and chlorite ranges in composition essentially from ripidolite to pychnochlorite (Fig. 5f). Titanite is common and often occurs as coronae around relict ilmenite. Fluorapatite, subhedral magnetite and chalcopyrite have been observed. A few scarce euhedral crystals of spinel, whose chemical composition varies between Al-chromite and picotite (sample Pil13: Fig. 5e; Table B in SM), are corroded and surrounded by coronae of Al-rich Cr-bearing chlorite (Pil13 in Table D; ripidolite in Fig. 5f), similarly to what is observed in serpentinites.

The major-element composition of the pillow lavas (Table G in SM) is highly variable, and the calculation of their C.I.P.W. norm gives irregular results. The normative composition of feldspars in particular is erratic and more often Ab-rich than An-rich ($An_{37\pm16}\ Ab_{57\pm18}\ Or_{6\pm3}$), which is manifested in the rocks by the changing behaviour of the original plagioclase phenocrysts, sometimes preserved and quite sodic (Pil13) or sometimes replaced by epidote pseudomorphs and thus initially Ca-rich (*e.g.*, Pil16). Such characteristics, in particular an enrichment in Na, can be attributed to some submarine weathering of the pillow lavas, which would therefore deserve the name “spilites” rather than “metabasalts”.

Foliated metabasites

In some foliated and banded metabasites (Fig. 7l), the deformation has destroyed all traces of the magmatic microstructures, making it difficult to diagnose what the original rock was, except when a transition with an undeformed metabasite is observed, which is sometimes the case in the vicinity of pillow lavas (Fig. 3e). These metabasites generally consist of a fine-grained assemblage of clinoamphibole (actinolite to magnesio-hornblende), chlorite (pychnochlorite), Fe^{3+}-rich epidote, albite (typically, $Ab_{99.8–96.6}$) sometimes coexisting with oligoclase, titanite, calcite, with some accessory minerals like apatite and magnetite surrounded by hematite. In one sample (Pil14), small crystals of phengite ($Ms_{56}Cel_{32}FeCel_5Pg_3Mrg_5$), with a significant phengitic $Si_{+1}Al^{IV}_{-1}Al^{VI}_{-1}(Mg, Fe)_{+1}$ substitution (Si = 6.525 ± 0.101 [1 σ] apfu), were observed.

Variations in the relative abundance of these minerals and grain size determine the banding. Fairly homogeneous ribbons, rich in calcite, in epidote (Fig. 7l) or more rarely in dolomite or quartz, seem to result from the transposition parallel to the foliation of early veinlets. In the

transposed veins of epidote, the latter is truncated and its gaps filled with albite and/or calcite (Fig. 7l). On the other hand, late veinlets of microcline intersect the foliation.

Radiolarite and calcschist

Metasediments, made up of metaradiolarites and calcschists, overlie stratigraphically the pillow-lavas. The gradual transition between these two formations is best seen on both sides of the gorge of Djendjene river where alternating layers of metaradiolarites, lavas and calcschists are observed (Fig. 3f).

Metaradiolarites, called "jaspéroïdes" by Durand-Delga (1955), deposited as 1- to 10-cm thick varicoloured beds. Reddish to greenish beds consists of quartz, ankerite ($Cal_{52}Mgs_{32}Sd_{15}Rds_{1}$) commonly concentrated in veinlets with nuclei of Fe-bearing dolomite ($Cal_{53}Mgs_{43}Sd_{4}Rds_{0}$), oxidized botryoidal pyrite, minute inclusions of clay, apatite and TiO_2. Whitish beds are composed of microcrystalline quartz with chalcedony cement. No radiolarian fossils were found in our samples due to intense recrystallisation. However, further west, in the Col de Chellata massif (Fig. 1), Gélard (1969) reported on the discovery in a red radiolarite layer of 21 radiolarian species of Late Jurassic (Kimmeridgian) age. This layer is located at the base of the Mauretanian flysch, in the same stratigraphic position as the Texenna metaradiolarites.

The calcschist beds range in thickness from a few decimetres to a few metres. Sample Cal consists of quartz, calcite ($Cal_{98}Mgs_{2}Sd_{0}$), dolomite ($Cal_{51}Mgs_{46}Sd_{3}$), chlorite, fluorapatite, hematite and white mica ($Ms_{63}Cel_{30}FeCel_{2}Pg_{4}Mrg_{1}$) with a significant phengitic substitution (Si = 6.654 ± 0.052 [1 σ] apfu).

Geochemistry

Most of the studied rocks have undergone a greenschist-facies metamorphism implying selective element mobility, especially for K, Na and the large ion lithophile elements (LILE: Cs, Rb, Ba, Sr....). For this reason, we use high field strength elements (HFSE: Ti, P, Zr, Y, Nb, Th…), some transition metals (*e.g.*, Ni, Co, Cr, V) and rare-earth elements (REE) in our geochemical and petrogenetic interpretations (Table G in SM), since these elements are identified as almost immobile during rock weathering and metamorphism in general, especially in the case of ophiolites (Pearce, 2014).

Loss-on-ignition (LOI) values of the serpentinite samples range from 11.8 to 13.6 wt.%. These elevated values are indeed due to hydration during serpentinization. The analysed serpentinites are highly magnesian (32.16–36.48 wt.% MgO) and have moderate Fe_{tot} concentrations ranging from 7.68 to 8.45 wt.% of Fe_2O_3. Their Mg number [Mg# = 100 × Mg^{2+} / (Mg^{2+} + Fe^{2+})] is elevated and varies from 90 to 92, which is typical of upper mantle peridotites. The Al_2O_3 and CaO concentrations are very low, ranging from 1 to 3.22 wt.% and from 0.04 to 1.54 wt.% respectively, in accordance with

418 the absence of plagioclase and the low amount of clinopyroxene in the harzburgite protolith (Fig. 6;
419 see above).

420 Metabasites show a wide range of LOI value (from 1.18 to 7.81 wt.%), which is lowest in
421 metadolerites and highest in metabasites with pillow-lava structures. This shows that the latter have
422 undergone an intensive alteration, as also indicated by the normative calculation (see above). The
423 metabasites have low SiO_2 and low to moderate TiO_2 contents, ranging from 44.6 to 49.2 wt.% and
424 from 1.05 to 2.17 wt.%, respectively. The MgO concentrations range from 3.47 to 9.29 wt.%, with the
425 lowest concentrations observed in the pillow lavas (3.47 to 3.81 wt.%). These low values do not
426 result from magmatic differentiation, but are rather due to the stronger alteration of the pillow-lava
427 samples. The metabasites display moderate Fe (7.41–11.75 wt.% of Fe_2O_3) and CaO (8.89–12.93
428 wt.%) contents and high Al_2O_3 (13.95–17.65 wt.%).

429 On the Zr/Ti vs. Nb/Y diagram (Pearce, 1996), the metabasites have basaltic subalkaline compositions
430 (Fig. 8a). Their tholeiitic nature is suggested by the Zr–P_2O_5 diagram (Floyd and Winchester, 1975)
431 used for distinguishing between alkaline and tholeiitic affinities (Fig. 8b), and by Zr–Y, La–Yb and Th–
432 Yb diagrams (Ross and Bédard, 2009) used for discriminating calc-alkaline and tholeiitic rocks (Fig. 8c-
433 e). In these latter three diagrams, some samples are plotted in the transitional field, a word used
434 here for rocks that plot at the tholeiitic/calc-alkaline boundary on the AFM diagram (Ross and
435 Bédard, 2009).

436 Chondrite-normalized REE patterns of the metabasites vary between two extremes (Fig. 9a, c, e). The
437 patterns of the metagabbro Mb9 and metadolerite Md5 show erratic variations probably due to
438 important secondary alteration and will not be considered hereafter. Pillow-lavas have nearly flat to
439 weakly depleted REE patterns with La_N/Yb_N ranging from 0.66 to 0.97 (Fig. 9a), whereas metagabbros
440 are enriched in Light REEs (LREE) with La_N/Yb_N ranging from 2.18 to 2.24, and show flat High REE
441 (HREE) profiles (Fig. 9e). The REE patterns of metadolerites are comparable to those of pillow lavas,
442 but with a slight enrichment in LREEs (La_N/Yb_N between 1.07 and 1.66: Fig. 9c). Thus, the REE patterns
443 of pillow-lavas, metadolerites and metagabbros are similar to those observed respectively in normal
444 middle-ocean ridge basalts (N-MORBs), transitional T-MORBs and enriched E-MORBs (*e.g.*, Gale et al.,
445 2013).

446 The same characteristics are shown in the N-MORB-normalized trace-element patterns (Fig. 9b, d, f),
447 in which pillow-lava samples are very close to 1 (with a slight Nb-Ta depletion) indicating their N-
448 MORB affinity whereas the metagabbros show E-MORB patterns.

449 # Discussion

Petrogenetic evolution of the Texenna ophiolites

Protoliths and geodynamic context

As pointed out above, the REE and multielement patterns of the Texenna metabasites correspond mainly to N-MORB for the pillow lavas, T-MORB for the metadolerites and E-MORB for the metagabbros. We use hereafter some discrimination diagrams to further refine the type of oceanic environment in which the rocks studied were formed.

In the V vs. Ti discrimination diagram (Shervais, 1982), most Texenna metabasic rocks plot in the MORB/back-arc basin basalt (BABB) fields (Ti/V = 18–48; Fig. 10a). On the Nb–Zr–Y diagram (Meschede, 1986), the pillow lava samples plot in the field of N-type MORB, metadolerites in within-plate tholeiites (WPT) and volcanic-arc basalt (VAB) fields, whereas metagabbros plot in E-MORB field (Fig. 10b). All the samples plot in the oceanic basalt domain of the La/10–Y/15–Nb/8 discrimination diagram of Cabanis and Lecolle (1989) (Fig. 10c), which defines also the pillow lava samples as N-MORB, the metagabbros as E-MORB and the metadolerite rocks as E-MORB falling between the pillow lavas and the metagabbros (Fig. 10c). The same results are seen in the Th–Ta–Hf/3 diagram of Wood (1980), where pillow-lava and Md6 metadolerite samples plot in N-MORB field, and other metadolerites and metagabbros in E-MORB field (Fig. 10d).

In recent years, powerful diagrams to fingerprint tectonic settings of ophiolites have become available (Pearce, 2008, 2014). These include the Th/Yb vs. Nb/Yb diagram where rocks from mid-ocean ridge and ocean island basalts (OIB) are plotted diagonally along a MORB-OIB array, and the Nb/Yb vs. TiO_2/Yb diagram, which allows discriminating between different types of MORBs. In the Th/Yb vs. Nb/Yb diagram, the Texenna mafic rocks plot within the MORB-OIB array (Fig. 10e), whereas in the Nb/Yb vs. TiO_2/Yb diagram pillow lavas are clearly N-MORB in character and metagabbros are E-MORB (Fig. 10f).

Discrimination diagrams corroborate an oceanic crust affinity of the studied metabasites, with N-MORB signature for the pillow lava samples, T-MORB for metadolerites and E-MORB for metagabbros. Furthermore, the association in the Texenna area of serpentinite, metagabbros, metadolerites, pillow lavas, radiolarites and calcschists is indeed typical of ophiolites, formed in an oceanic environment. Following the classification scheme of Dilek and Furnes (2011, 2014), these may be classified as subduction-unrelated ophiolites that evolved during rift drift and seafloor spreading.

Greenschist-facies hydrothermal oceanic metamorphism

Despite complete serpentinization, Texenna serpentinites very commonly show microstructures inherited from the original peridotites, such as serpentine pseudomorphs after olivine (*i.e.*, mesh texture) and pseudomorphs after orthopyroxene (*i.e.*, bastite), in which even traces of former exsolution lamellae are still visible. Their mineralogical composition is characterized by lizardite in both mesh textures and bastites, magnetite, "ferritchromit" with chlorite coronae replacing former Cr-spinel, and small veins of chrysotile and chlorite. All these textural and mineralogical features, in particular the alteration of Cr-spinel (*e.g.*, Burkhard, 1993; Mellini et al., 2005; Kapsiotis et al., 2007), are well documented in ophiolite serpentinites. They are also typical of the ocean floor serpentinites, the hydrothermal serpentinization of which occurs in the range of 300–500°C (Mével, 2003).

Metadolerites, metagabbros and pillow lavas are weakly deformed since they have preserved their magmatic microstructures, only intersected by fractures filled with albite, epidote and/or calcite. Their mineral assemblages, with albite, chlorite, epidote, titanite and actinolite, are typical of greenschist-facies metamorphic alteration of basic rocks. Thompson (1991), in particular, described such alteration of pillowed basalts in the dredged metabasalts from the ocean floor. Furthermore, most of the chlorites from the Texenna metabasites plot in the field corresponding to greenschist-facies seafloor hydrothermal alteration in the Si vs. Fe/(Fe+Mg) diagram (Fig. 5f; see Nimis et al., 2004, and references therein).

In summary, many rocks of Texenna, either serpentinites, metabasites or pillow lavas, have preserved the original texture of their protolith and are therefore weakly deformed. The magmatic minerals of the protoliths were very generally replaced by low-grade greenschist-facies hydrous metamorphic assemblages, accompanied by secondary mineral precipitation in veins and fractures. These features are typical of hydrothermal oceanic metamorphism, during which strain is reduced to fracturing, under temperatures in the range of 300–500°C (Hekinian, 1982; Mével, 2003). The abundance of carbonates, both in metasediments (calcschists and ankerite-bearing radiolarites) and as veinlets in metabasites, indicates that this hydrothermalism occurred above the carbonate compensation depth.

Metamorphism and deformation related to the Maghrebide orogen

Some of the Texenna metabasites are deformed, showing prominent banding and foliation (see above). The foliation of these rocks is sub-parallel to the foliation in the neighbouring geological formations, such as the Kabyle basement, the associated calcschists and the Massylian flysch, so the deformation appears to be related to the tectonic emplacement of these units, well after the oceanic hydrothermal metamorphism. The mineralogy of these metabasites is not fundamentally different from that of undeformed metabasites, metamorphosed under greenschist-facies hydrothermal

514 oceanic conditions. One notable difference, however, appears to be the presence of phengite (Pil14),
515 also observed in some calcschists (sample Cal); this relatively high-*P* mineral cannot have formed
516 under sub-surface conditions during the hydrothermal oceanic metamorphism.

517 Specifying the *P-T* conditions of this metamorphism is not as simple as it seems. While modelling a *P-*
518 *T* pseudosection requires ideally a homogeneous rock that has reached equilibrium, most of these
519 rocks are banded and may have preserved minerals from the oceanic hydrothermal metamorphic
520 stage and even from the magmatic protolith, like ilmenite in the core of titanite crystals; they are
521 also crosscut by late calcite and feldspar veinlets, which have modified the bulk composition. We
522 have chosen to model a *P-T* pseudosection for the Pil14 metabasite, derived from pillow lavas but
523 strongly deformed and foliated during this metamorphism. The chemical composition used for the
524 modelling, including the Fe^{3+} content, was obtained from the molar modal quantities of the minerals
525 in the rock, calculated by the least-square method from the bulk-rock and mineral compositions, and
526 from which apatite and calcite, not taken into account in the model, were subtracted. Low albite (Ab)
527 was considered in addition to plagioclase (Pl), since the "peristerite" miscibility gap can occur in such
528 a low-grade metamorphism. Details on the thermodynamic database and solid-solution models are
529 given in Section 5 of the SM.

530 The *P-T* conditions of the metamorphism related to deformation should correspond to one of the
531 fields where the minerals ubiquitous in the rock are stable (Ab, Ep, Chl, Act/Hbl, Tnt, Ms/Ph,
532 ±hematite), *i.e.*, in the vicinity of the low-*P*–low-*T* / high-*P*–high-*T* diagonal of the *P-T* pseudosection
533 (Fig. 11). Glaucophane-bearing high-*P*–low-*T* fields should be excluded, since this mineral was never
534 observed, as well as the low-*P*–high-*T* fields in which epidote is absent and plagioclase too An-rich
535 ($An_{21–38}$) relative to the real values. Because of the banding and heterogeneity of the rock, the use of
536 isopleths is somewhat hazardous. However, the Si-in-phengite isopleths (Si = 6.525 ± 0.101 [±1σ])
537 make it possible to better specify the *P-T* domain for this metamorphism (Fig. 11). The stability of
538 some Kfs predicted by the model is in agreement with the presence of late veinlets of K-feldspar. It
539 therefore appears that the metamorphism linked to the tectonic emplacement of the Texenna
540 ophiolites in the Maghrebide chain occurred under low-grade greenschist-facies conditions, following
541 a medium geothermal gradient that is not linked to a subduction zone.

542 ## Comparison with other ophiolites of the western Mediterranean region

543 Numerous ophiolitic outcrops occur in the Alpine orogen of the Western Mediterranean region, *e.g.*,
544 in the Alps, in North-eastern Corsica, in the Northern and Southern Apennines, in Sicily, in the Rif
545 (Morocco) and in the Betic Cordillera (southern Spain) (Principi et al., 2004; Bortolotti and Principi,

2005; Guerrera et al., 2005). These ophiolites are considered to represent the records of the Jurassic Western Tethys Ocean, and are characterized by the following features (Principi et al., 2004): (i) Middle-Late Jurassic age; (ii) MORB signature of the mafic rocks; (iii) reduced and thin ophiolitic successions; (iv) exposure of serpentinites at the base of sedimentary-volcanic covers; and (v) widespread presence of radiolarites above the magmatic section. It is prominent to note that all of these features can be seen in the Texenna volcano-sedimentary complex.

Recently, ophiolite slivers with gabbros, altered basalts and oceanic sediments have been discovered in the core of the external zones of the Central Rif belt in Morocco, far from the Maghrebian Flysch suture zone (Benzaggagh et al., 2014; Michard et al., 2014). These rocks define two major lineaments in the Mesorif (Michard et al., 2018; Fig. 1): (i) The Mesorif suture zone (MSZ) shows slivers of serpentinites, metagabbros, metabasalts, associated with oceanic metasediments. A gabbro of the MSZ gave a radiometric age of 190 Ma (Michard et al., 2018). (ii) The Mesorif Basalts–Breccias lineament (MBB), composed of Kimmeridgian–Berriasian basalt flows and carbonates breccias, is more external and parallel to the MSZ.

The metabasic rocks of Alpine ophiolites of the Western Mediterranean region show compositions from N-MORB to E-MORB:

(a) In the Chenaillet ophiolitic complex (Ligurian-Piemonte zone in the Western Alps), the mafic rocks are predominantly N-MORB (Chalot-Prat, 2005) and this complex, as well as other Western Alpine ophiolites exposed in NW Italy, is considered as the testimony of a segment of an axial volcanic ridge in a slow-spreading ridge within a restricted ocean basin (Balestro et al., 2019; Chalot-Prat, 2005).

(b) Two groups of ophiolites are distinguished in Corsica (Saccani et al., 2008): (i) a most prevalent group with N-MORB affinity and (ii) a group with T-MORB composition restricted to Santo di Tenda, Nebbio and upper part of Balagne units. The N-MORB group is considered to have been formed in the central part of the ocean after the onset of the oceanic spreading, whereas the T-MORB rocks would have originated in the ocean-continent transition zone during the first stage of oceanic spreading.

(c) The metabasites of the ophiolitic sequences of the Calabrian Arc (Southern Apennines) have N-MORB (Sansone et al., 2011) to T-MORB tholeiitic affinities (Liberi et al., 2006).

(d) In Sicily and Moroccan Rif, the metabasites show E-MORB characteristics (Durand-Delga et al., 2000) and are thought to be formed in a rift environment during the initial stage of oceanisation (Durand-Delga et al., 2000).

(e) The metabasites of the Betic ophiolites show mainly E-MORB or T-MORB affinities (Bodinier et al., 1987; Puga et al., 2011). They are interpreted as formed in ultraslow-spreading ridge environment, during the initial stages of oceanisation, and are classified as "continental margin ophiolites" (Puga et al., 2017). The Betic oceanic sector was located at the westernmost end of the Western Tethys Ocean. However, a few authors proposed a continental setting for the metabasic igneous rocks of the Betics (*e.g.*, Gomez-Pugnaire, 2019, and references therein).

In Th/Yb vs. Nb/Yb diagram, the Texenna pillow lavas, with N-MORB affinity, lie mainly within the Chenaillet and most of the Corsica mafic rocks array (Fig. 12), whereas metagabbros and metadolerites show affinities with mafic ophiolitic rocks of the Rif, Sicily, the Betics and with the recently studied metabasites of Eastern Elba Island (Northern Apennines, Italy; Bianco et al., 2019) (Fig. 12). Finally, the Kimmeridgian–Berriasian basalts of the MBB and the gabbros of the MSZ of the Central Rif belt in Morocco show E-MORB affinities and differ from the Texenna metabasites, in the Th/Yb–Nb/Yb discrimination diagram (Fig. 12). The gabbros of the MSZ plot between E-MORB and OIB, while basalts of the MBB plot above the MORB-OIB array, with high Th/Yb ratios probably due to interaction of these basalts with crustal rocks of the African palaeomargin (Benzaggagh et al., 2014).

The Texenna serpentinites share the same features as many Alpine ophiolitic serpentinites, like those at Chenaillet (Thiéblemont et al., 2019): high serpentinization degree; lizardite as serpentine polymorph; alteration of Cr-spinel to "ferritchromit" surrounded by chlorite coronae; harzburgite protolith. On the other hand, the studied serpentinites differ notably from the Collo peridotites and serpentinites, which crop out within the metamorphic basement of Lesser Kabylia not far from the Texenna area. Collo ultramafic rocks are much less serpentinized than those of Texenna, with antigorite instead of lizardite as the dominant serpentine polymorph; they display anhydrous mineral assemblages, unaltered Cr-spinels and their protolith is lherzolitic (Laouar et al., 2017). Collo ultramafic rocks belong to Alpine-type peridotites that were emplaced within an orogenic setting (Bouillin and Kornprobst, 1974; Laouar et al., 2017) and are similar to other peridotite massifs of the Western Mediterranean region: Lherz (Pyrenees); Lanzo massif (Italian Alps); Ronda (Betic Cordillera); and Beni Bousera (the Moroccan Rif).

Geodynamic implications

This study demonstrates for the first time that the Texenna rocks belong to a true ophiolitic slice. Contrary to what has been suggested by some authors, the Maghrebian Flysch suture zone is marked by outcrops of ophiolites, as any other suture zone of the Circum-Mediterranean Alpine Belts, and the sedimentary cover of the Flysch domain was here deposited over a true oceanic rather than a

609 thinned continental crust. The Texenna ophiolites show analogies with other ophiolites from the
610 Western Mediterranean region, indicating that they are remnants of the ancient oceanic domain
611 formed in the southwestern part of the Western Tethys (Fig. 13a), more precisely in the Maghrebian
612 Tethys ocean that developed between Africa and Iberia during the Middle-Late Jurassic (*e.g.*,
613 Fernandez, 2019).

614 The Texenna metabasites show T-MORB to E-MORB affinities for the metadolerites and metagabbros
615 and N-MORB signature for the pillow lavas. This can be interpreted in two ways:

616 (a) The pillow lavas and the intrusive rocks are coeval and were emplaced in the same area, which is
617 supported by the association of N-MORB to E-MORB basalts in modern ultraslow-spreading ridge,
618 such as the Southwest Indian Ridge (Standish et al., 2008). This however seems contradictory with
619 the harzburgite composition of the serpentinite protoliths, which would rather indicate a formation
620 at a fast-spreading ridge.

621 (b) The intrusive rocks are not coeval with the extrusive igneous rocks (*i.e.*, the pillow lavas). The
622 gabbros and dolerites may have emplaced at an early stage of oceanic accretion, which could explain
623 their enriched geochemical signature. After the onset of oceanic spreading, basaltic magmas with an
624 N-MORB affinity would have produced the pillow lavas observed.

625 The latter scenario, proposed for the Betic ophiolites (Puga et al., 2011), would apply well to the
626 Texenna ophiolites; it is similar to the tectonic models of the Alpine Tethys evolution developed by
627 Balestro et al. (2019) and of the Mesozoic margin evolution of the Maghrebian Tethys invoked by
628 Michard et al. (2020) for the Rif belt (Morocco). According to this model, the Alpine Tethys was
629 formed in four stages between the Middle Jurassic to Early Cretaceous involving seafloor spreading
630 of a narrow ocean basin: (1) emplacement of gabbro bodies and dolerite dykes in the upper mantle
631 peridotites; (2) extensional deformation, upper mantle exhumation-denudation and doming; (3)
632 eruption of basaltic lavas into the exhumed peridotites and gabbroic plutons and (4) deposit of
633 pelagic sediments (radiolarites, marble and calcschist). The emplacement of the intrusive rocks
634 (gabbros, dolerites) in the Texenna complex would correspond to the phase 1 of this model, in
635 accordance with their E-MORB affinity and association with serpentinite in the field. The pillow lavas
636 emplacement is likely related to phase 3, which would explain their N-MORB composition. Finally,
637 the overlying radiolarites are linked to phase 4.

638 Bouillin (1992) proposed that the Texenna rocks were close to a NW-SE Jurassic transform fault that
639 brought the Lesser Kabylia basement, to the NE, into direct contact with the Maghrebian oceanic
640 basin, to the SW (Fig. 13b). This hypothesis elegantly accounts for (a) the apparent dextral shift
641 between the continental basements of Lesser and Greater Kabylias, (b) the absence near Texenna of

642 the “Dorsale calcaire”, considered elsewhere as the remnant of the former southern passive margin
643 of the Kabyle microcontinent, and (c) the thrusting of the Lesser Kabylia basement directly upon the
644 ophiolites (Bouillin, 1992). This NW-SE transform fault would be one of the many later proposed by
645 Schettino and Turco (2011) in their palaeogeographic reconstruction of the western Tethys (Fig. 13a).

646 The Maghrebide orogeny partly deformed, metamorphosed and dismembered the ophiolites of
647 Texenna, the original sequence of which is hardly recognizable, with serpentinites, on the one hand,
648 and pillow lavas and metasediments, on the other hand, unclearly concentrated on the SW and NE
649 edges, respectively, of the tectonic slice.

650 Ophiolitic outcrops are much less common in the Maghrebide chain of North Africa than in other
651 regions. A possible reason for the extreme scarcity of ophiolite remnants in the Maghrebian Flysch
652 suture zone is the fact that the basement of the Maghrebian Flysch nappes is rooted deeply beneath
653 the internal zone. Furthermore, the geological formations at the front of the internal zones are highly
654 dilacerated and dismembered, which led to the dispersion in the suture zone of the different units of
655 the ophiolitic sequence into slivers, separated by long distances.

656 These ophiolite slivers were often considered in ancient literature as part of the metamorphic
657 basement, like the Texenna rocks, long regarded as belonging to the Kabyle basement. Since the
658 suture(s) zone(s) of the Maghrebide chain is(are) usually outlined by Triassic outcrops, they were also
659 frequently mistaken for Triassic "ophites" (*e.g.*, Ben Yaich et al., 1989). The mafic and ultramafic
660 rocks that crop out in the core of the external zones of the Central Rif belt, supposed until recently to
661 be basement units or Triassic ophites, have been recognized as part of Middle-Upper Jurassic
662 ophiolite slivers, defining a second suture zone within the Maghrebide chain, between the Intrarif
663 and Mesorif (External Zones, Morocco) (Benzaggagh et al., 2014). A major challenge for the future is
664 therefore to investigate magmatic-sedimentary associations, very little studied so far, which could
665 reveal new sutures in the Maghrebide chain.

666 Conclusions

667 (i) An association of mafic and ultramafic rocks occurs beneath the Maghrebian flysch nappes at
668 the southern front of the internal zones of Lesser Kabylia, in the Texenna region (NE Algeria).
669 This association includes serpentinite, metagabbro, metadolerite, metabasalt with pillow-lava
670 structures, and oceanic metasediments (radiolarite and calcschists).
671 (ii) Serpentinites are mainly composed of lizardite pseudomorphs after olivine and
672 orthopyroxene, with small veins of chrysotile and chlorite scattered throughout the rocks.

673 Metadolerites and metagabbros have sometimes preserved their magmatic zoned plagioclase
674 (labrador to andesine), but are generally transformed into an assemblage of albite,
675 actinolite/magnesio-hornblende, epidote, chlorite and titanite, in the same way as the
676 metabasalts, which furthermore commonly show inherited microstructures typical of pillow
677 lavas (concentric former glassy, variolitic and spherulitic zones; recrystallized devitrification
678 spherulites; epidote pseudomorphs after plagioclase phenocrysts; gas vesicles filled with
679 epidote and chlorite). The greenschist-facies static metamorphism that affected the Texenna
680 metabasites and serpentinites is typical of hydrothermal alteration of ocean floor rocks at
681 slow-spreading ridges. After the oceanic hydrothermal metamorphism, the Texenna
682 ophiolites underwent some deformation accompanied by greenschist-facies phengite-bearing
683 metamorphism, linked to the tectonic emplacement of the ophiolites in their current setting
684 during the Maghrebide orogen.

685 (iii) Whole-rock compositions of the serpentinites indicate a harzburgite protolith, whereas the
686 metabasic rocks are tholeiitic and show N-MORB signature for the pillow-lavas and from T-
687 MORB to E-MORB affinities for the intrusive rocks (metadolerites and metagabbros). This
688 duality is common among the ophiolites of the western Mediterranean region.

689 (iv) This study demonstrates for the first time that the Texenna rocks belong to a true ophiolitic
690 slice, and indicates that the sedimentary cover of the Maghrebian Flysch domain was
691 deposited over a true oceanic rather than a thinned continental crust, as several researchers
692 often suggest. The Texenna ophiolites represent a fragment of the ancient oceanic
693 lithosphere (Maghrebian Tethys Ocean) that formed between Africa and Iberia-AlKaPeCa
694 during the Middle-Upper Jurassic.

695 # Acknowledgments

696 We would like to warmly thank Jean-Pierre Bouillin for his invaluable advices, especially concerning
697 the metabasites and pillow lavas of the Tabellout region, as well as the head office of the Tabellout
698 dam for allowing us to access the outcrops. Grateful thanks are also due to the *Direction Générale de*
699 *la Recherche Scientifique et du Développement Technologique* for funding this work. Moulley Charaf
700 Chabou is supported by the *Ministère de l'Enseignement Supérieur et de la Recherche Scientifique*,
701 PRFU project n°E04N01UN190120180001. André Michard and an anonymous reviewer are sincerely
702 thanked for their constructive reviews, as well as Marco Scambelluri for the editorial handling.

703 # Bibliography

Andrieux, J., Djellit, H., 1989. Structure de la Petite Kabylie occidentale (Algérie): flyschs «ultra» et flyschs externes. Comptes rendus de l'Académie des sciences, Série II, 309, 1191–1196.

Andrieux, J., Frizon de Lamotte, D., Braud, J., 1989. A structural scheme for the western Mediterranean area in Jurassic and Early Cretaceous times. Geodinamica Acta 3, 5–15.

Arndt, N., Fowler, A., 2004. Textures in komatiites and variolitic basalts, in: Eriksson, P.G., Altermann, W., Nelson, D.R., Mueller, W.U., Catuneanu, O. (Eds.), The Precambrian Earth: tempos and events. Elsevier, Developments in Precambrian Geology 12, pp. 298–311.

Balestro, G., Festa, A., Dilek, Y., 2019. Structural architecture of the Western Alpine Ophiolites, and the Jurassic seafloor spreading tectonics of the Alpine Tethys. Journal of the Geological Society 176, 913–930.

Baudelot, S., Bouillin, J.-P., Coiffait, P., 1981. Découverte d'Ordovicien inférieur daté par Acritarches dans l'Ouest de la Petite Kabylie: conséquences structurales. Comptes Rendus de l'Académie des Sciences 293, 611–614.

Ben Yaich, A., Hervouët, Y., Duée, G., El Hatimi, N., Aubouin, J., 1989. Age jurassique et réinterprétation des roches basiques au Nord de Ouezzane (Rif externe, Maroc); signification géodynamique. Comptes rendus de l'Académie des sciences. Série 2, 309, 1197–1202.

Benzaggagh, M., Mokhtari, A., Rossi, P., Michard, A., El Maz, A., Chalouan, A., Saddiqi, O., Rjimati, E.-C., 2014. Oceanic units in the core of the External Rif (Morocco): Intramargin hiatus or South-Tethyan remnants? Journal of Geodynamics 77, 4–21.

Bianco, C., Godard, G., Halton, A., Brogi, A., Liotta, D., Caggianelli, A., 2019. The lawsonite-glaucophane blueschists of Elba Island (Italy). Lithos 348-349, 105–198.

Bodinier, J.-L., Morten, L., Puga, E., de Federico, A.D., 1987. Geochemistry of metabasites from the Nevado-Filabride Complex, Betic Cordilleras, Spain: Relics of a dismembered ophiolitic sequence. Lithos 20, 235–245.

Bortolotti, V., Principi, G., 2005. Tethyan ophiolites and Pangea break-up. Island Arc 14, 442–470.

Bouillin, J., 1974. Présence de flyschs Maurétaniens épimétamorphiques dans le massif du Moul Ed Demamène (Constantinois, Algérie). Comptes Rendus de l'Académie des Sciences, Série D, 279, 1059–1062.

Bouillin, J.-P., 1979. La transversale de Collo et d'El Milia (Petite Kabylie): une région-clef pour l'interprétation de la tectonique alpine de la chaîne littorale d'Algérie. Mémoires de la Société Géologique de France (nouv. s.) 135, 83 p.

Bouillin, J.-P., 1986. Le "bassin maghrébin"; une ancienne limite entre l'Europe et l'Afrique à l'ouest des Alpes. Bulletin de la Société géologique de France (8ème s.) 2, 547–558.

Bouillin, J.-P., 1989. La suture alpine en Méditerranée occidentale. Remarques sur une synthèse et rappel d'une autre conception. II: réponses. Bulletin de la Société géologique de France (8ème s.) 5, 859–567.

Bouillin, J.-P., 1992. La répartition des affleurements de la Dorsale kabyle: héritage d'une segmentation mésozoïque de la marge nord-téthysienne? Comptes rendus de l'Académie des sciences, Série 2, 315, 1127–1132.

Bouillin, J.-P., Hernandez, J., 1975. Découverte de roches volcaniques associées aux phtanites cénomaniennes du flysch massylien dans le Nord du Constantinois (Algérie). Compte rendu sommaire des séances de la Société géologique de France 17, 14–16.

Bouillin, J.-P., Kornprobst, J., 1974. Associations ultrabasiques de Petite Kabylie: péridotites de type alpin et complexe stratifié; comparaison avec les zones internes bético-rifaines. Bulletin de la Société géologique de France (7ème s.) 16, 183–194.

Bouillin, J.-P., Durand-Delga, M., Gélard, J.P., Leikine, M., Raoult, J.F., Raymond, D., Tefiani, M., Vila, J.M., 1970. Définition d'un flysch massylien et d'un flysch maurétanien au sein des flyschs allochtones de l'Algérie. Comptes Rendus de l'Académie des Sciences 270, 2249–2252.

Bouillin, J.-P., Kornprobst, J., Raoult, J.F., 1977. Données préliminaires sur le complexe volcano-sédimentaire de Rekkada Metletine (ex-Texenna), en Petite Kabylie (Algérie). Bulletin de la Société géologique de France (7ème s.) 19, 805–813.

Burkhard, D.J.M., 1993. Accessory chromium spinels: Their coexistence and alteration in serpentinites. Geochimica et Cosmochimica Acta 57, 1297–1306.

Cabanis, B., Lecolle, M., 1989. Le diagramme La/10–Y/15–Nb/8: un outil pour la discrimination des séries volcaniques et la mise en évidence des processus de mélange et/ou de contamination crustale. Comptes Rendus de l'Académie des Sciences, Série 2, 309, 2023–2029.

Chalot-Prat, F., 2005. An undeformed ophiolite in the Alps: Field and geochemical evidence for a link between volcanism and shallow plate tectonic processes, in: Fouger, G.R., Natland, J.H.,

764 Presnall, D.C., Anderson, D.L. (Eds.), Plates, Plumes, and Paradigms. Geological Society of
765 America special Paper 388, pp. 751–780.

766 Chalouan, A., Michard, A., El Kadiri, Kh., Negro, F., Frizon de Lamotte, D., Soto, J.I., Saddiqi, O., 2008.
767 The Rif Belt, in: Michard, A., Saddiqi, O., Chalouan, A., Frizon de Lamotte, D. (Eds.),
768 Continental Evolution: The Geology of Morocco. Springer, Lecture Notes in Earth Sciences
769 116, pp. 203–302.

770 Coutelle, A., Gélard, J.P., 1968. Existence de radiolarites à la base du "flysch schisto-gréseux
771 tithonique-néocomien" du col de Chellata (Grande Kabylie). Compte rendu sommaire des
772 séances de la Société géologique de France 3, 79–81.

773 Coutelle, A., Delteil, J., 1989. La suture alpine en Méditerranée occidentale. Remarques sur une
774 synthèse et rappel d'une autre conception. Bulletin de la Société géologique de France (8ème
775 s.) 5, 859–867.

776 Dilek, Y., Furnes, H., 2011. Ophiolite genesis and global tectonic fingerprinting of ancient oceanic
777 lithosphere. The Geological Society of America Bulletin 123, 387–411.

778 Dilek, Y., Furnes, H., 2014. Ophiolites and their origins. Elements 10, 93–100.

779 Djellit, H., 1987. Évolution tectono-métamorphique du socle kabyle et polarité de mise en place des
780 nappes de flysch en Petite Kabylie occidentale (Algérie). Thèse de Doctorat, Université Paris
781 XI, 206 p.

782 Durand-Delga, M., 1948. Sur la structure du Moul ed Demamène (Chaîne Numidique, Algérie).
783 Comptes Rendus de l'Académie des Sciences 226, 1826–1827.

784 Durand-Delga, M., 1949. Notes sur la structure géologique des environs de Texenna (Petite Kabylie,
785 Algérie). Bulletin de la Société géologique de France (5ème s.) 19, 271–278.

786 Durand-Delga, M., 1950. Le chevauchement bordier de Petite Kabylie (Algérie). Comptes Rendus de
787 l'Académie des Sciences 231, 1522–1524.

788 Durand-Delga, M., 1954. Les rapports des venues doléritiques du Mouled-Demamene (chaine
789 Numidique, Algérie) et de la mise en place de la nappe bordière de Petite Kabylie. XIXème
790 Congrès géologique international, Alger, 1952, fasc. XVII, C. R. section XV, 37–41.

791 Durand-Delga, M., 1955. Etude géologique de l'Ouest de la chaîne numidique. Bulletin du Service de
792 la Carte Géologique de l'Algérie, 2ème série, Stratigraphie-Descriptions régionales 24, 533 p.

793 Durand-Delga, M., 1971. Les unités à Mésozoïque métamorphique d'El Milia à Texenna (Algérie) et
794 leur cadre structural. Bulletin de la Société géologique de France (7ème s.) 13, 328–337.

795 Durand-Delga, M., Fontobé, J.M., 1980. Le cadre structural de la Méditerranée occidentale. 26ème
796 Congrès Géol. Int. Paris, Coll. 5. Mémoires du BRGM 115, 67–87.

797 Durand-Delga, M., Rossi, P., Olivier, P., Puglisi, D., 2000. Situation structurale et nature ophiolitique
798 de roches basiques jurassiques associées aux flyschs maghrébins du Rif (Maroc) et de Sicile
799 (Italie). Comptes Rendus de l'Académie des Sciences, Série IIA 331, 29–38.

800 Ehrmann, E.F., 1946. Feuille au 50000e « Tamesguida », avec notice explicative. Service de la Carte
801 géologique de l'Algérie, Alger.

802 Fernandez, O., 2019. The Jurassic evolution of the Africa-Iberia conjugate margin and its implications
803 on the evolution of the Atlantic-Tethys triple junction. Tectonophysics 750, 379–393.

804 Floyd, P.A., Winchester, J.A., 1975. Magma type and tectonic setting discrimination using immobile
805 elements. Earth and Planetary Science Letters 27, 211–218

806 Frizon de Lamotte, D., Raulin, C., Mouchot, N., Wrobel-Daveau, J.-C., Blanpied, C., Ringenbach, J.-C.,
807 2011. The southernmost margin of the Tethys realm during the Mesozoic and Cenozoic:
808 Initial geometry and timing of the inversion processes. Tectonics 30, TC3002, doi:
809 10.1029/2010TC002691.

810 Furnes, H., Safonova, I., 2019. Ophiolites of the Central Asian Orogenic Belt: Geochemical and
811 petrological characterization and tectonic settings. Geoscience Frontiers 10, 1255–1284.

812 Gale, A., Dalton, C.A., Langmuir, C.H., Su, Y., Schilling, J.G., 2013. The mean composition of ocean
813 ridge basalts. Geochemistry, Geophysics, Geosystems 14, 489–518.

814 Gélard, J.P., 1969. Le flysch à base schisto-gréseuse de la bordure méridionale et orientale du massif
815 de Chellata; le flysch maurétanien (Grande-Kabylie, Algérie). Bulletin de la Société
816 Géologique de France (7ème s.) 11, 676–686.

817 Gomez-Pugnaire, M.T., Sanchez-Vizcaino, V.L., Fernandez-Soler, J.M., Acosta-Vigil, A., 2019. Mesozoic
818 and Cenozoic magmatism in the Betics, in: Quesada, C., Oliveira, J.T. (Eds.), The Geology of
819 Iberia: a geodynamic approach, Vol. 3: The alpine cycle. Springer, Regional Geology
820 Reviews, pp. 545–566.

821 Guerrera, F., Martín-Martín, M., Perrone, V., Tramontana, M., 2005. Tectono-sedimentary evolution
822 of the southern branch of the Western Tethys (Maghrebian Flysch Basin and Lucanian
823 Ocean): consequences for Western Mediterranean geodynamics. Terra Nova 17, 358–367.

824 Hawthorne, F.C., Oberti, R., Harlow, G.E., Maresch, W.V., Martin, R.F., Schumacher, J.C., Welch, M.D.,
825 2012. Nomenclature of the amphibole supergroup. American Mineralogist 97, 2031–2048.

826 Hekinian, R., 1982. Petrology of the Ocean Floor. Elsevier Oceanography Series 33, Elsevier, Academic
827 Press, 393 p.

828 Hey, M.H., 1954. A new review of the chlorites. Mineralogical Magazine and Journal of the
829 Mineralogical Society 30, 277–292.

830 Holland, T.J.B., Powell, R., 2011. An improved and extended internally consistent thermodynamic
831 dataset for phases of petrological interest, involving a new equation of state for solids.
832 Journal of Metamorphic Geology 29, 333–383.

833 Kapsiotis, A., Tsikouras, B., Grammatikopoulos, T., Karipi, S., Hatzipanagiotou, H., 2007. On the
834 metamorphic modification of Cr-spinel compositions from the ultrabasic rocks of the Pindos
835 ophiolite complex (NW Greece). Bulletin of the Geological Society of Greece 40, 781–793.

836 Laouar, R., Satouh, A., Salmi-Laouar, S., Abdallah, N., Cottin, J.-Y., Bruguier, O., Bosch, D., Ouabadi, A.,
837 Boyce, A.J., Fallick, A.E., 2017. Petrological, geochemical and isotopic characteristics of the
838 Collo ultramafic rocks (NE Algeria). Journal of African Earth Sciences 125, 59–72.

839 Le Bas, M.J., Streckeisen, A.L., 1991. The IUGS systematics of igneous rocks. Journal of the Geological
840 Society 148, 825–833.

841 Leprêtre, R., Frizon de Lamotte, D., Combier, V., Gimenos-Vives, O., Mohn, G., Eschard, R., 2018. The
842 Tell-Rif orogenic system (Morocco, Algeria, Tunisia) and the structural heritage of the
843 southern Tethys margin. BSGF-Earth Sciences Bulletin 189, 10,
844 doi.org/10.1051/bsgf/2018009.

845 Liberi, F., Morten, L., Piluso, E., 2006. Geodynamic significance of ophiolites within the Calabrian Arc.
846 Island Arc 15, 26–43.

847 Mellini, M., Rumori, C., Viti, C., 2005a. Hydrothermally reset magmatic spinels in retrograde
848 serpentinites: formation of “ferritchromit” rims and chlorite aureoles. Contributions to
849 Mineralogy and Petrology 149, 266–275.

Meschede, M., 1986. A method of discriminating between different types of mid-ocean ridge basalts and continental tholeiites with the Nb–Zr–Y diagram. Chemical Geology 56, 207–218.

Mével, C., 2003. Serpentinization of abyssal peridotites at mid-ocean ridges. Comptes rendus Geoscience 335, 825–852.

Michard, A., Mokhtari, A., Chalouan, A., Saddiqi, O., Rossi, P., Rjimati, E.-C., 2014. New ophiolite slivers in the External Rif belt, and tentative restoration of a dual Tethyan suture in the western Maghrebides. Bulletin de la Société géologique de France 185, 313–328.

Michard, A., Mokhtari, A., Lach, P., Rossi, P., Chalouan, A., Saddiqi, O., Rjimati, E.-C., 2018. Liassic age of an oceanic gabbro of the External Rif (Morocco): Implications for the Jurassic continent–ocean boundary of Northwest Africa. Comptes Rendus Geoscience 350, 299–309.

Michard, A., Saddiqi, O., Chalouan, A., Chabou, M.C., Lach, P., Rossi, P., Bertrand, H., Youbi, N., 2020. Comment on "The Mesozoic Margin of the Maghrebian Tethys in the Rif Belt (Morocco): Evidence for Polyphase Rifting and Related Magmatic Activity" by Gimeno-Vives et al. Tectonics 39, e2019TC006004.

Nimis, P., Tesalina, S.G., Omenetto, P., Tartarotti, P., Lerouge, C., 2004. Phyllosilicate minerals in the hydrothermal mafic–ultramafic-hosted massive-sulfide deposit of Ivanovka (southern Urals): comparison with modern ocean seafloor analogues. Contributions to Mineralogy and Petrology 147, 363–383.

Pearce, J.A., 1996. A user's guide to basalt discrimination diagrams. Geological Association of Canada Special Publication 12, 79–113.

Pearce, J.A., 2008. Geochemical fingerprinting of oceanic basalts with applications to ophiolite classification and the search for Archean oceanic crust. Lithos 100, 14–48.

Pearce, J.A., 2014. Immobile element fingerprinting of ophiolites. Elements 10, 101–108.

Principi, G., Bortolotti, V., Chiari, M., Cortesogno, L., Gaggero, L., Marcucci, M., Saccani, E., Treves, B., 2004. The pre-orogenic volcano-sedimentary covers of the western Tethys oceanic basin: a review. Ofioliti 29, 177–211.

Puga, E., Fanning, M., De Federico, A.D., Nieto, J.M., Beccaluva, L., Bianchini, G., Díaz Puga, M.A., 2011. Petrology, geochemistry and U–Pb geochronology of the Betic Ophiolites: Inferences for Pangaea break-up and birth of the westernmost Tethys Ocean. Lithos 124, 255–272.

879 Puga, E., De Federico, A.D., Fanning, M., Nieto, J.M., Martínez-Conde, J.A.R., Díaz Puga, M.A., Lozano,
880 J.A., Bianchini, G., Natali, C., Beccaluva, L., 2017. The Betic Ophiolites and the Mesozoic
881 Evolution of the Western Tethys. Geosciences 7, 31, doi: 10.3390/geosciences7020031.

882 Raoult, J.-F., 1974. Géologie du centre de la chaîne numidique: Nord du Constantinois, Algérie.
883 Mémoires de la Société géologique de France (nouv. s.) 121, 1-162 + dépliants.

884 Reynard, B., 2013. Serpentine in active subduction zones. Lithos 178, 171–185.

885 Roman'ko, E.F., Roman'ko, A.E., Meskhi, A.M., 1998. The geology and geochemistry of Meso-
886 Cenozoic magmatic formations in Northeastern Algeria. Doklady Earth Sciences 362, 925–
887 927.

888 Ross, P.-S., Bédard, J.H., 2009. Magmatic affinity of modern and ancient subalkaline volcanic rocks
889 determined from trace-element discriminant diagrams. Canadian Journal of Earth Sciences
890 46, 823–839.

891 Saccani, E., Principi, G., Garfagnoli, F., Menna, F., 2008. Corsica ophiolites: geochemistry and
892 petrogenesis of basaltic and metabasaltic rocks. Ofioliti 33, 187–207.

893 Sansone, M.T.C., Rizzo, G., Mongelli, G., 2011. Petrochemical characterization of mafic rocks from the
894 Ligurian ophiolites, southern Apennines. International Geology Review 53, 130–156.

895 Schettino, A., Turco, E., 2011. Tectonic history of the western Tethys since the Late Triassic. The
896 Geological Society of America Bulletin 123, 89–105.

897 Shervais, J.W., 1982. Ti-V plots and the petrogenesis of modern and ophiolitic lavas. Earth and
898 Planetary Science Letters 59, 101–118.

899 Standish, J.J., Dick, H.J., Michael, P.J., Melson, W.G., O'Hearn, T., 2008. MORB generation beneath
900 the ultraslow spreading Southwest Indian Ridge (9–25°E): Major element chemistry and the
901 importance of process versus source. Geochemistry Geophysics Geosystems 9, Q05004,
902 doi.org/10.1029/2008GC001959.

903 Sun, S.S., McDonough, W.F., 1989. Chemical and isotopic systematics of oceanic basalts: Implications
904 for mantle composition and processes. Geological Society of London, Special Publication 42,
905 313–345.

906 Thiéblemont, D., Duron, J., Plunder, A., 2019. Atlas pétrographique obstiné de l'ophiolite du
907 Chenaillet. Géologie de la France 2019 (4), 1–78; http://geolfrance.brgm.fr/mise-en-ligne-
908 dun-atlas-petrographique-roches-massif-chenaillet-brianconnais-hautes-alpes.

909 Thompson, G., 1991. Metamorphic and hydrothermal processes: basalt-seawater interactions, in:
910 Floyd, P.A. (Ed.), Oceanic basalts. Springer, New York, pp. 148–173.

911 Wildi, W., 1983. La chaîne tello-rifaine (Algérie, Maroc, Tunisie): structure, stratigraphie et évolution
912 du Trias au Miocène. Revue de Géographie physique et de Géologie dynamique 24, 201–
913 297.

914 Wood, D.A., 1980. The application of a Th Hf Ta diagram to problems of tectonomagmatic
915 classification and to establishing the nature of crustal contamination of basaltic lavas of the
916 British Tertiary Volcanic Province. Earth and Planetary Science Letters 50, 11–30.

917 # Figure Captions

918 **Fig. 1.** Betic-Maghrebian Chain (modified from Chalouan et al., 2008) with the location of mafic rocks
919 with ophiolite affinities associated to the flysch zone.

920 **Fig. 2.** Geological overview of the Texenna region (Lesser Kabylia). **(a)** Geological map compiled from
921 Durand-Delga (1955), Andrieux and Djellit (1989) and original geological survey; S_0: stratification in
922 flysch and sediments; S_1: foliation or schistosity in metamorphic rocks. **(b)** Panoramic view from
923 36°39'33"N–5°46'25"E, before the filling of the Tamellout dam, showing the contacts between the
924 Kabyle basement (KB), the ophiolite complex (Sendouah-Tabellout Unit: STU) and the flysch domain
925 (FD).

926 **Fig. 3.** Outcrop photographs of the Texenna ophiolite complex. **(a)** Metadolerite vein crosscutting the
927 serpentinite**. (b)** Chrysotile veinlets in serpentinite**. (c)** Metadolerite dyke inside calcschists. **(d)**
928 Metagabbroic rock mainly composed of chlorite (Chl), epidote (Ep) and actinolite (Act), intersected
929 by whitish veins of calcite (Cal) and quartz (Qz). **(e)** Pillow lava showing a massive nucleus of
930 porphyritic metabasalt, surrounded by greenish, aphyritic and schistose rims. **(f)** Alternating layers of
931 radiolarite and metabasalt on top of the pillow lavas. **(g)** Pillows with deformed ellipsoidal shapes. **(h)**
932 Pillow lava with external chlorite-rich and variolitic zones. Outcrops are at Djebel Es-Sendouah (a-b),
933 Tabellout (c-d) and Oued Djendjene gorge, near the Tabellout water dam (e-h).

934 **Fig. 4.** Petrology and microstructures of serpentinite. **(a)** Serpentine (Srp) mesh texture, bastite and
935 altered chromite (Chr). **(b)** Detail of the mesh microstructure showing cells derived from olivine
936 grains, with an edge rich in tiny crystals of magnetite (Mag) enveloping concentric layers of
937 serpentine. **(c)** Detail of the bastite microstructure showing tremolite (Tr) grooves in serpentine
938 (dashed arrow), interpreted as former Cpx lamellae exsolved in the Opx protocrystal. **(d)** Altered
939 chromite grains surrounded by a chlorite (Chl) corona, and intersected by late veinlets of tremolite

and/or chlorite. BSE images (a-c) and (d) composite EDS elemental map of Fe (red), Cr (green) and Al (blue).

Fig. 5. Mineral compositions in serpentinites and metabasites. **(a-c)** Calcic clinoamphiboles in the metabasites, following the nomenclature of Hawthorne et al. (2012). **(d)** Feldspars in the metabasites. The inset rectangle shows the composition profile A–B across a magmatic plagioclase in metadolerite Md4; the red line indicates the position of the Carlsbad twin plane on this profile, whose position is shown in Figure 7d-e; chemical analyses are given in Table C of SM (2: rim, core, rim). **(e)** Composition of Cr-spinels and their pseudomorphs, in serpentinites and metabasalts. **(f)** Compositions of chlorites from serpentinites and metabasites in the classification diagram of Hey (1954). "Sea floor hydrothermally altered rocks" from Nimis et al. (2004).

Fig. 6. Ol–Cpx–Opx normative molar composition of the studied serpentinites, following the nomenclature of Le Bas and Streckeisen (1991).

Fig. 7. Petrology and microstructures of the metabasites. **(a-c)** Greenschist-facies metabasite, with albite (Ab), epidote (Ep), actinolite (Act), hornblende (Hbl), chlorite (Chl) and titanite (Tnt), showing the preserved doleritic texture of the gabbroic protolith crosscut by albite and epidote veins. **(d-e)** Metadolerite, showing the still-preserved magmatic laths of plagioclase in a matrix of actinolite (Act) and pargasite (Prg); A–B: composition profile across plagioclase (see Fig. 5d). **(f-k)** Microstructures of the pillow lavas (see text for the meaning of the Z1–Z4 and 1–5 labels; to be compared with Fig. B in SM); (f) pillow zoning (Z1, chlorite-rich outer zone after glassy crust; Z2 and Z3, variolitic zones, rich in former devitrification spherulites; Z4, internal massive zone); (g) preserved magmatic flow in the outer zone; (h) epidote pseudomorph after plagioclase phenocrysts; (j) epidote+albite association after devitrification spherulites, around former plagioclase microliths; (k) microgeode after gas bubble, filled with epidote, clinozoisite and chlorite. **(l)** Deformed metabasite, with early transposed veins of calcite (Cal) and truncated epidote (Ep+Ab), and late veins of K-feldspar (Kfs). SEM images (a, c, d, g-j, l) and composite BSE and EDS elemental maps of Al, Ca, Fe, and Ti (b, e-f, k).

Fig. 8. Geochemical discrimination diagrams of the metabasites. Red squares: pillow lava samples (Pil12-13-14-15); green diamonds: metadolerite samples (Md4-5-6); blue circles: metagabbro samples (Mb9-10-11); ppm means µg/g. **(a)** Zr/Ti vs. Nb/Y diagram (Pearce, 1996). **(b)** P_2O_5 vs. Zr diagram (Floyd and Winchester, 1975). **(c)** Zr vs. Y; **(d)** La vs. Yb and **(e)** Th vs. Yb diagrams (Ross and Bédard, 2009).

Fig. 9. REE and trace-element patterns for the metabasites. **(a, c, e)** Chondrite-normalized REE patterns and **(b, d, f)** N-MORB-normalized incompatible-element patterns. (a, b) Pillow lavas; (c, d) metadolerites; (e, f) metagabbros. The normalizing values for chondrites and N-MORB are from Sun

973 and McDonough (1989) and Gale et al. (2013), respectively. N-MORB and E-MORB compositions are
974 from Gale et al. (2013).

975 **Fig. 10.** Tectonic setting discrimination diagrams. Red squares: pillow lava samples (Pil12-13-14-15);
976 green diamonds: metadolerite samples (Md4-5-6); blue circles: metagabbro samples (Mb9-10-11)**.**
977 **(a)** Ti vs. V diagram of Shervais (1982). **(b)** Zr/4–2Nb–Y discrimination diagram of Meschede (1986);
978 WPA: within-plate alkali basalts; WPT: within-plate tholeiites; VAB: volcanic-arc basalts. **(c)** Y/15–
979 La/10–Nb/8 discrimination diagram of Cabanis and Lecolle (1989). **(d)** Th–Hf/3–Ta discrimination
980 diagram (Wood, 1980). **(e)** Th/Yb vs. Nb/Yb and **(f)** TiO_2/Yb vs. Nb/Yb diagrams (Pearce, 2008).

981 **Fig. 11.** *P-T* pseudosection modelled for the composition of the Pil14 metabasite. The minerals are
982 listed in decreasing order of abundance, those in brackets being in negligible quantity (< 2 vol.%).
983 Since the sample was subjected to deformation and metamorphism during the emplacement of the
984 ophiolites in the Maghrebide belt, the model applies to this episode.

985 **Fig. 12.** Th/Yb vs. Nb/Yb diagram showing the compositional fields of some ophiolites of the Western
986 Mediterranean region. (1) Kimmeridgian–Berriasian basalt flows of the Mesorif Basalts–Breccias
987 lineament (MBB) and (2) Bou Adel gabbros of the Mesorif suture zone (MSZ) (Morocco) (Benzaggagh
988 et al., 2014); (3) Metabasites of the Betic ophiolites (Puga et al., 2011); (4) Metabasites of Eastern
989 Elba Island (Northern Apennines, Italy) (Bianco et al., 2019); (5) Metabasic rocks of the Chenaillet
990 ophiolitic complex (Western Alps) (Chalot-Prat, 2005); (6) Metabasic rocks of Alpine Corsica
991 ophiolites (Saccani et al., 2008).

992 **Fig. 13.** The western Tethys at the Upper Jurassic. **(a)** Palaeogeographic reconstruction after
993 Schettino and Turco (2011). NPF: North Pyrenean Fault; GiF: Gibraltar Fault; red lines: middle-ocean
994 ridges; orange lines: rifts. **(b)** Schematic reconstruction of the north-tethysian margin of the Kabylias
995 after Bouillin (1992).

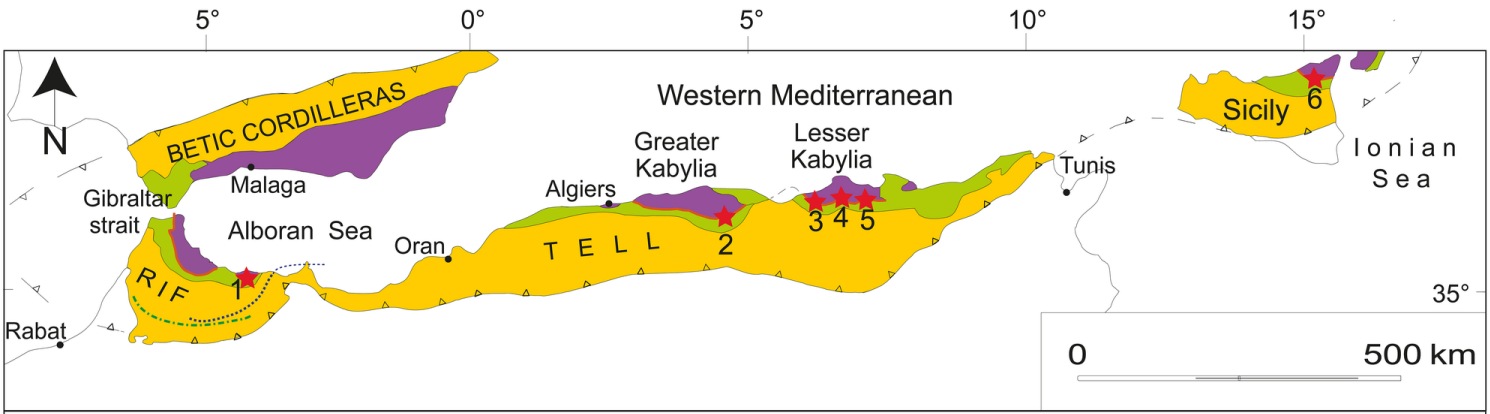
5°
0°
5°
10°
15°
N
BETIC CORDILLERAS
Western Mediterranean
Sicily
6
Ionian Sea
Greater Kabylia
Lesser Kabylia
Gibraltar strait
Malaga
Algiers
Tunis
Alboran Sea
Oran
T E L L
2
3 4 5
R I F
1
35°
Rabat
0
500 km
External Zones
Flysch Nappes
Internal Zones
Maghrebian Flysch suture zone
Mafic/ultramafic rocks (ophiolites)
Mesorif suture zone (MSZ)
Mesorif Basalts-Breccias lineament (MBB)
1 Northern Rif (Morocco)
2 Chellata massif (Algeria)
3 Texenna (Algeria; this study)
4 Moul ed Damamène (Algeria)
5 Fedj el Mekta' (Algeria)
6 Sicily (Italy)

Figure 1

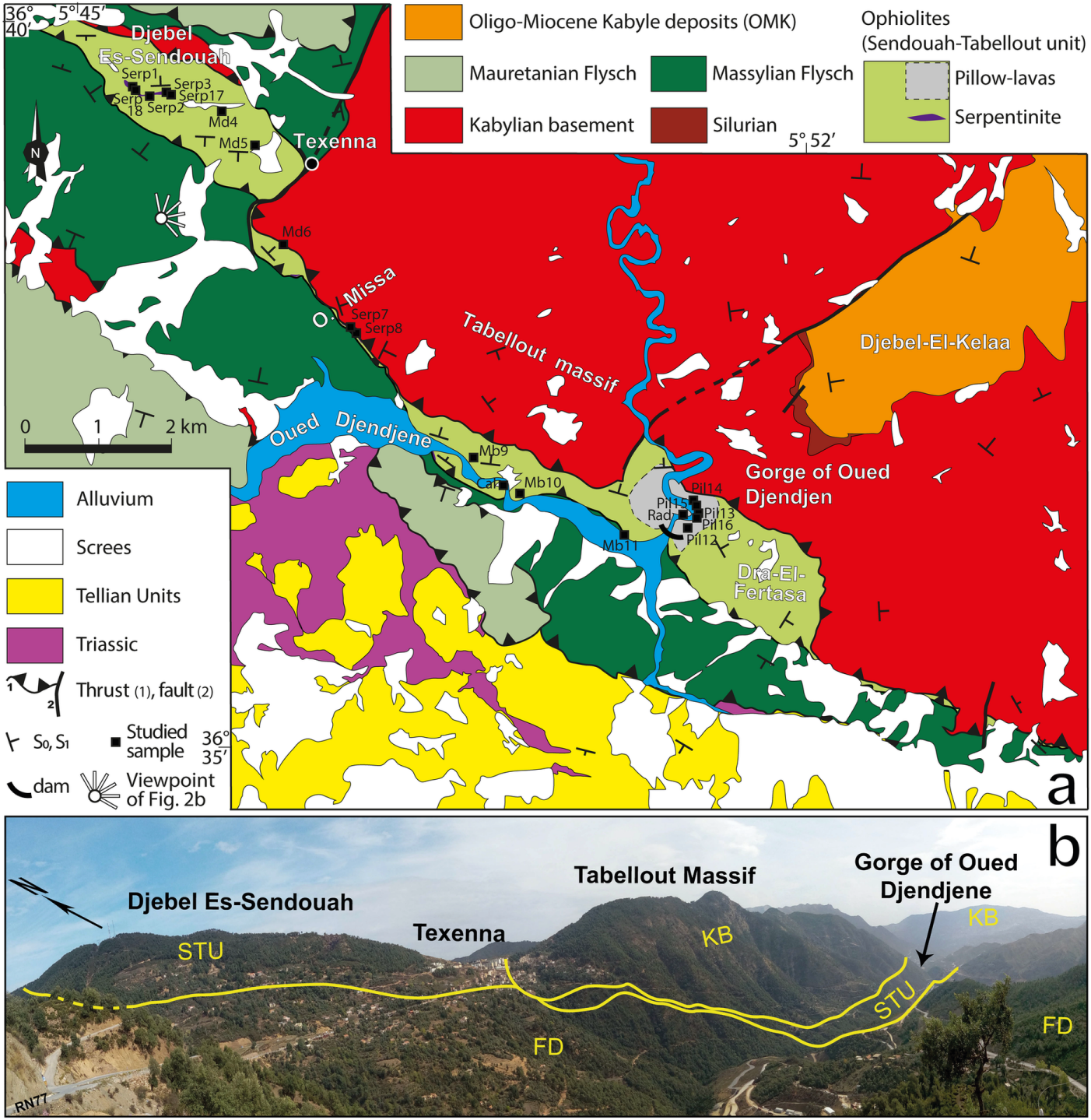
36° 40′
5° 45′
Djebel Es-Sendouah
Serp1
Serp3
Serp17
Serp 18
Serp2
Md4
Md5
Texenna
N
Md6
O. I-Missa
Serp7
Serp8
Tabellout massif
Djebel-El-Kelaa
0
1
2 km
Oued Djendjene
Mb9
Cal1
Mb10
Pil14
Pil15
Rad
Pil13
Pil16
Pil12
Mb11
Gorge of Oued Djendjen
Dra-El-Fertasa
5° 52′
36° 35′
Oligo-Miocene Kabyle deposits (OMK)
Mauretanian Flysch
Massylian Flysch
Kabylian basement
Silurian
Ophiolites (Sendouah-Tabellout unit)
Pillow-lavas
Serpentinite
Alluvium
Screes
Tellian Units
Triassic
Thrust (1), fault (2)
S0, S1
Studied sample
dam
Viewpoint of Fig. 2b
a
b
Djebel Es-Sendouah
STU
Texenna
Tabellout Massif
KB
Gorge of Oued Djendjene
KB
STU
FD
FD
RN77

Figure 2

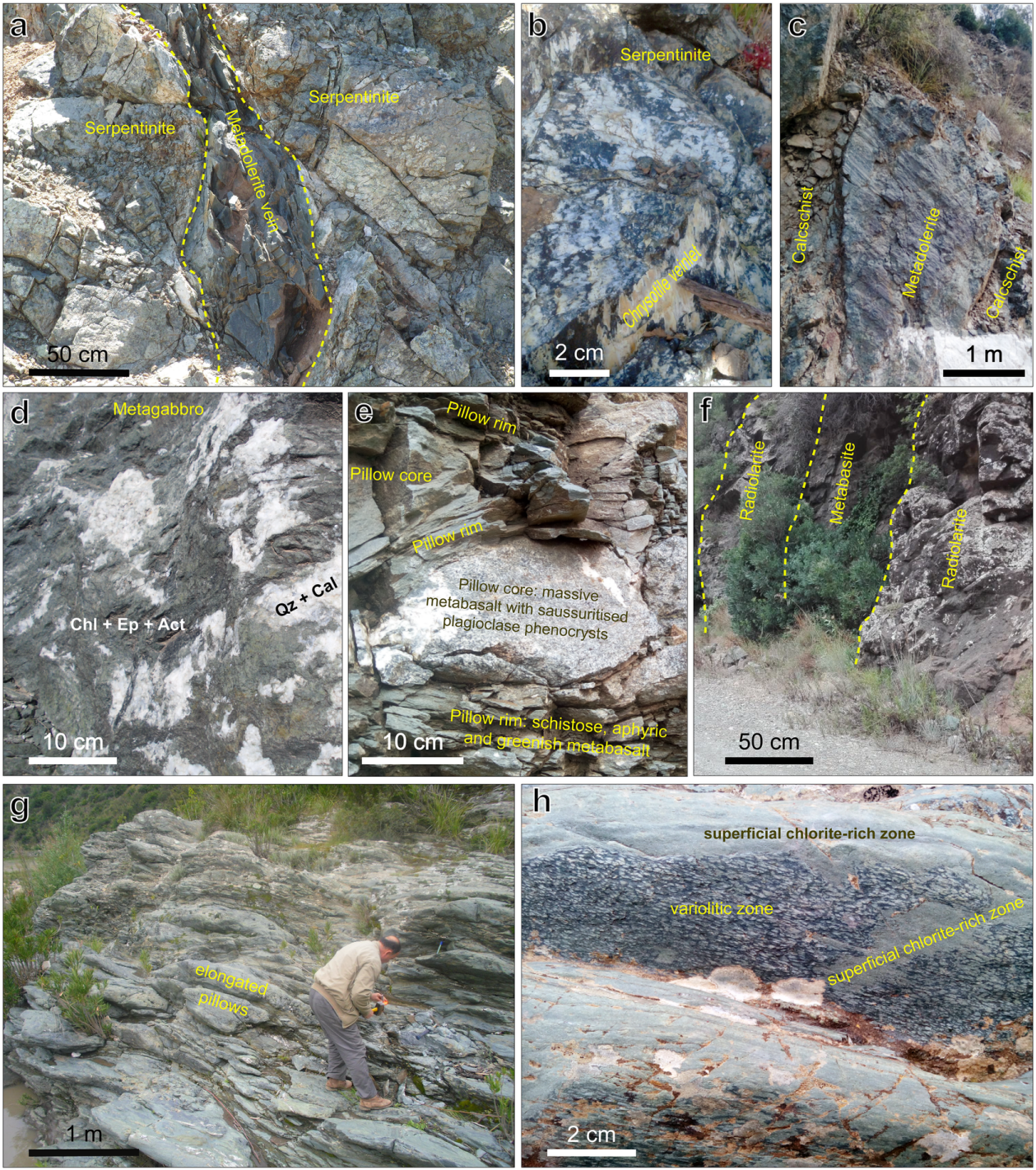
a
Serpentinite
Serpentinite
Mafic dolerite vein
50 cm
b
Serpentinite
Chrysotile veinlet
2 cm
c
Calcschist
Metadolerite
Calcschist
1 m
d
Metagabbro
Chl + Ep + Act
Qz + Cal
10 cm
e
Pillow rim
Pillow core
Pillow rim
Pillow core: massive metabasalt with saussuritised plagioclase phenocrysts
Pillow rim: schistose, aphyric and greenish metabasalt
10 cm
f
Radiolarite
Metabasite
Radiolarite
50 cm
g
elongated pillows
1 m
h
superficial chlorite-rich zone
variolitic zone
superficial chlorite-rich zone
2 cm

Figure 3

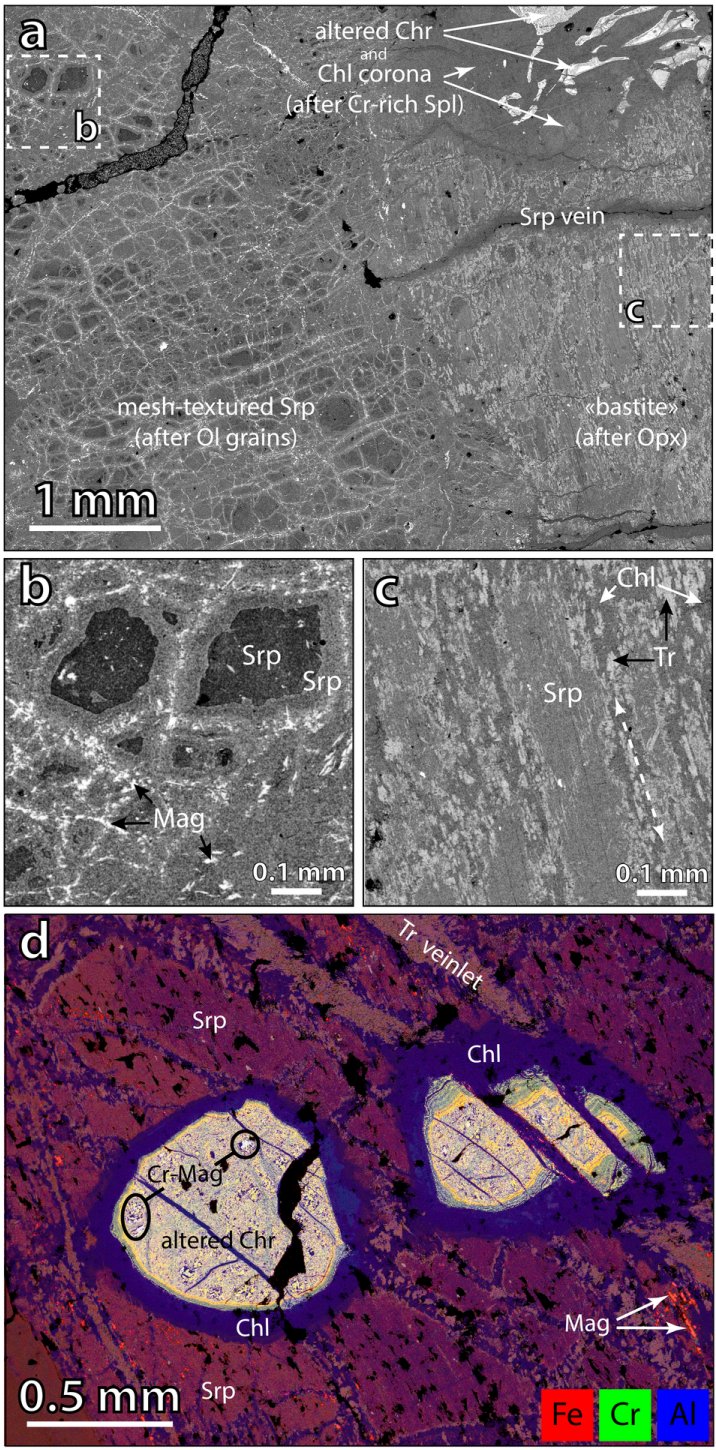
a
altered Chr
and
Chl corona
(after Cr-rich Spl)
b
Srp vein
c
mesh-textured Srp
(after Ol grains)
«bastite»
(after Opx)
1 mm
b
Srp
Srp
Mag
0.1 mm
c
Chl
Tr
Srp
0.1 mm
d
Tr veinlet
Srp
Chl
Cr-Mag
altered Chr
Chl
Mag
0.5 mm
Srp
Fe
Cr
Al

Figure 4

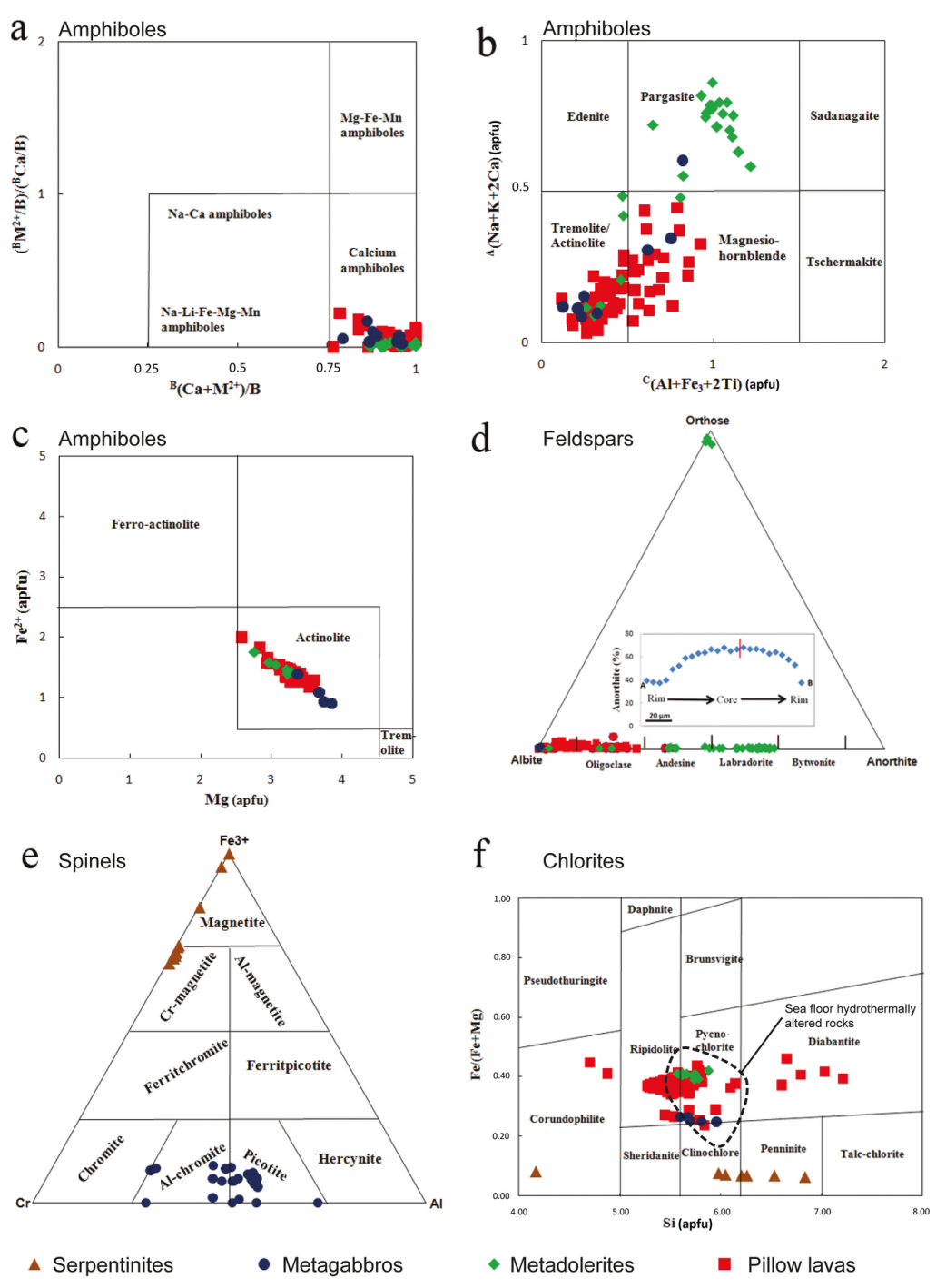
a
Amphiboles
Mg-Fe-Mn amphiboles
Na-Ca amphiboles
Calcium amphiboles
Na-Li-Fe-Mg-Mn amphiboles
(BM2+/B)/(BCa/B)
B(Ca+M2+)/B
b
Amphiboles
Edenite
Pargasite
Sadanagaite
Tremolite/ Actinolite
Magnesio-hornblende
Tschermakite
A(Na+K+2Ca) (apfu)
C(Al+Fe3+2Ti) (apfu)
c
Amphiboles
Ferro-actinolite
Actinolite
Trem-olite
Fe2+ (apfu)
Mg (apfu)
d
Feldspars
Orthose
Albite
Oligoclase
Andesine
Labradorite
Bytwonite
Anorthite
Anorthite (%)
Rim
Core
Rim
20 μm
e
Spinels
Fe3+
Magnetite
Cr-magnetite
Al-magnetite
Ferritchromite
Ferritpicotite
Chromite
Al-chromite
Picotite
Hercynite
Cr
Al
f
Chlorites
Daphnite
Brunsvigite
Pseudothuringite
Sea floor hydrothermally altered rocks
Pycno-chlorite
Ripidolite
Diabantite
Corundophilite
Sheridanite
Clinochlore
Penninite
Talc-chlorite
Fe/(Fe+Mg)
Si (apfu)
Serpentinites
Metagabbros
Metadolerites
Pillow lavas

Figure 5

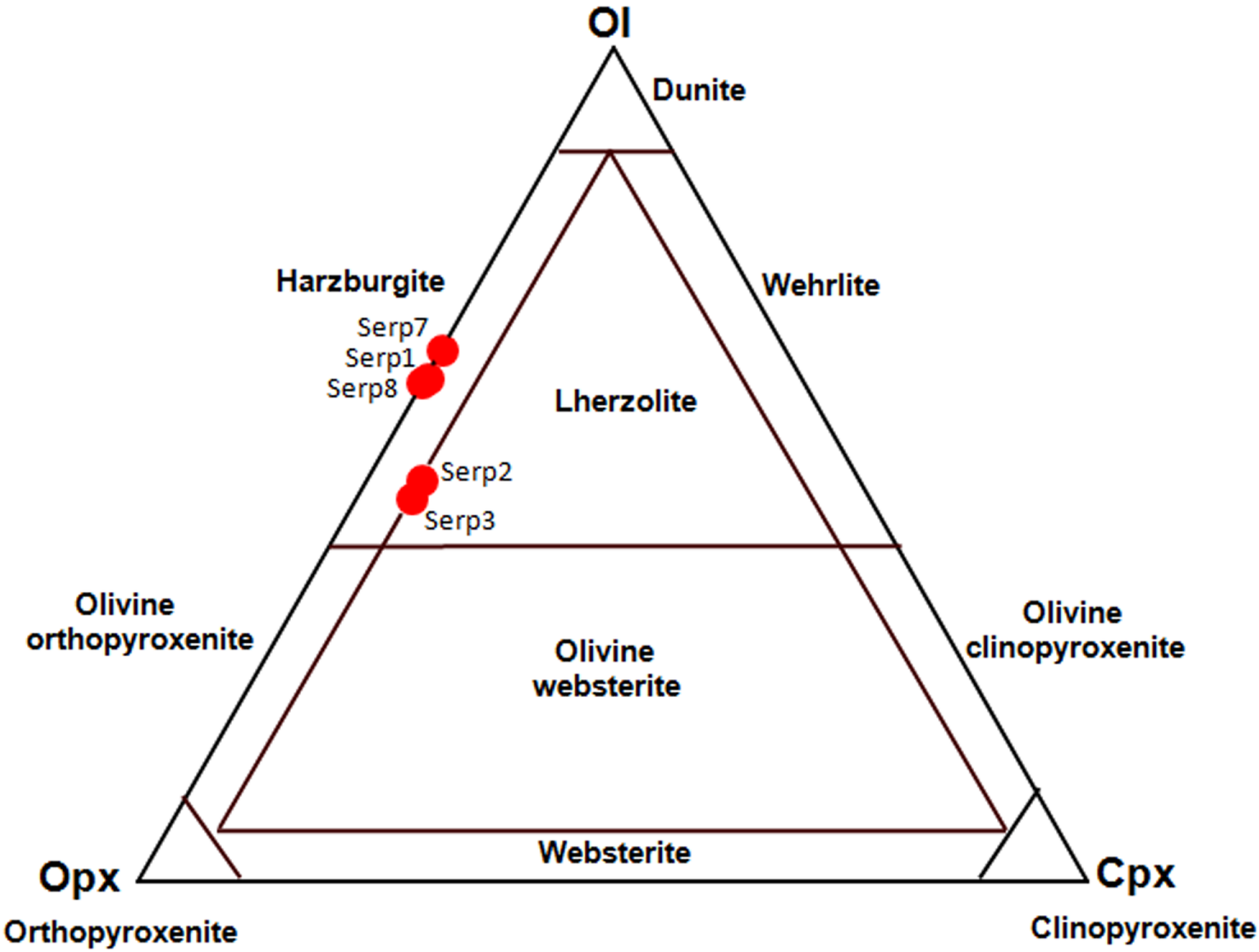
Ol
Dunite
Harzburgite
Wehrlite
Serp7
Serp1
Serp8
Lherzolite
Serp2
Serp3
Olivine
orthopyroxenite
Olivine
clinopyroxenite
Olivine
websterite
Websterite
Opx
Cpx
Orthopyroxenite
Clinopyroxenite

Figure 6

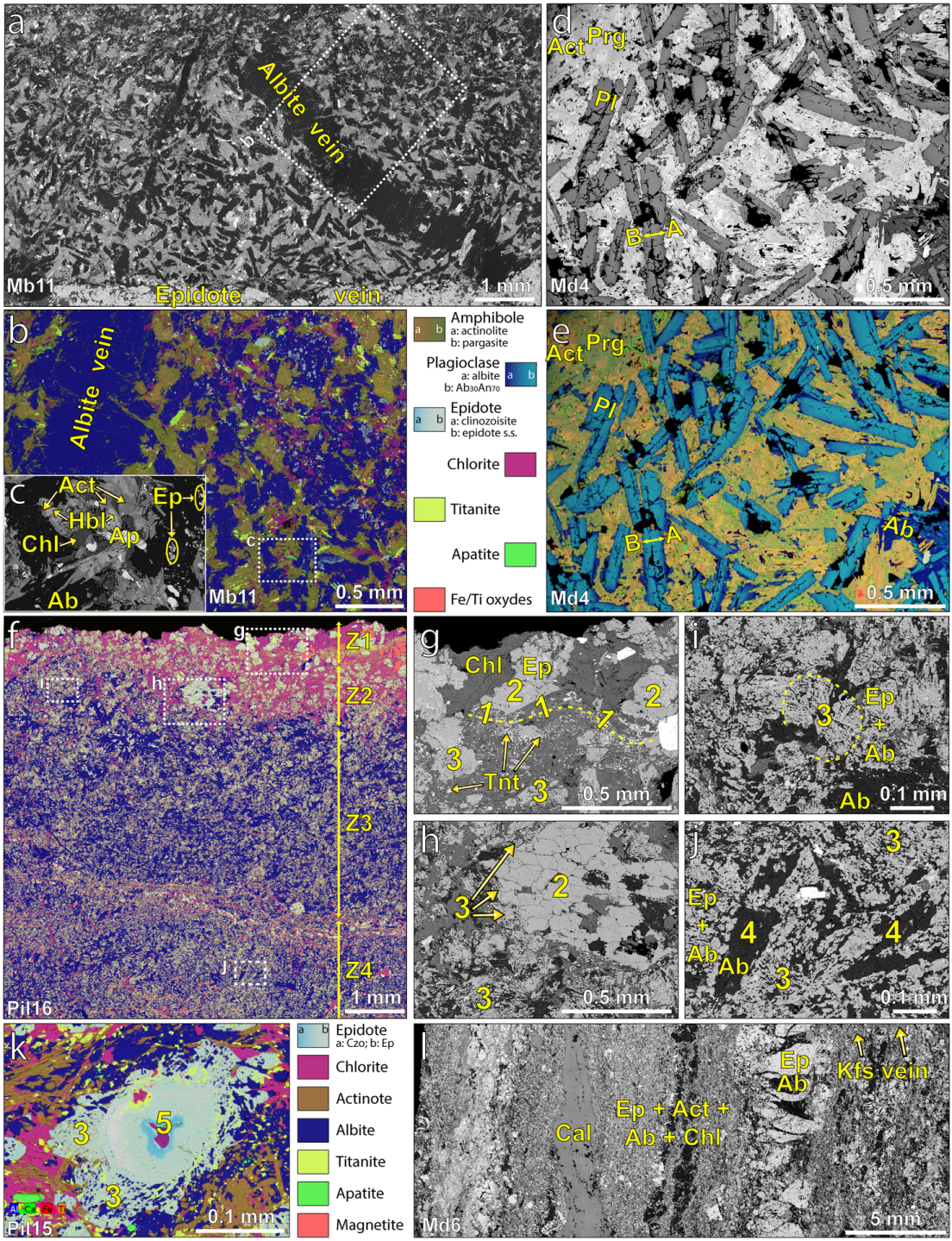
a
Albite vein
b
Mb11
Epidote vein
1 mm
d
Act
Prg
Pl
B
A
Md4
0.5 mm
b
Albite vein
c
Act
Hbl
Chl
Ep
Ap
Ab
Mb11
0.5 mm
Amphibole
a: actinolite
b: pargasite
Plagioclase
a: albite
b: Ab30An70
Epidote
a: clinozoisite
b: epidote s.s.
Chlorite
Titanite
Apatite
Fe/Ti oxydes
e
Act
Prg
Pl
B
A
Ab
Md4
0.5 mm
f
g
h
i
j
Z1
Z2
Z3
Z4
Pil16
1 mm
g
Chl
Ep
2
1
3
Tnt
0.5 mm
i
Ep
+
Ab
3
Ab
0.1 mm
h
2
3
3
0.5 mm
j
3
Ep
+
Ab
4
4
Ab
3
0.1 mm
k
3
5
3
Pil15
0.1 mm
Epidote
a: Czo; b: Ep
Chlorite
Actinote
Albite
Titanite
Apatite
Magnetite
l
Ep
Ab
Kfs vein
Cal
Ep + Act +
Ab + Chl
Md6
5 mm

Figure 7

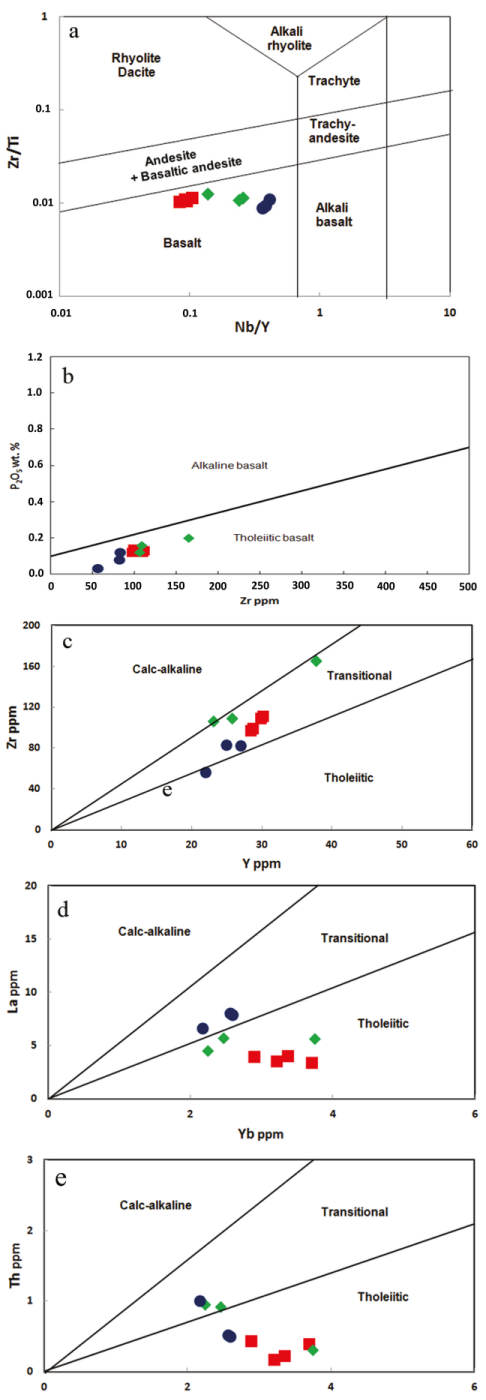
a
Alkali rhyolite
Rhyolite Dacite
Trachyte
Trachy-andesite
Andesite + Basaltic andesite
Alkali basalt
Basalt
Zr/Ti
Nb/Y
b
Alkaline basalt
Tholeiitic basalt
P_2O_5 wt.%
Zr ppm
c
Calc-alkaline
Transitional
Tholeiitic
Zr ppm
Y ppm
d
Calc-alkaline
Transitional
Tholeiitic
La ppm
Yb ppm
e
Calc-alkaline
Transitional
Tholeiitic
Th ppm
Yb ppm
Metagabbros
Metadolerites
Pillow lavas

Figure 8

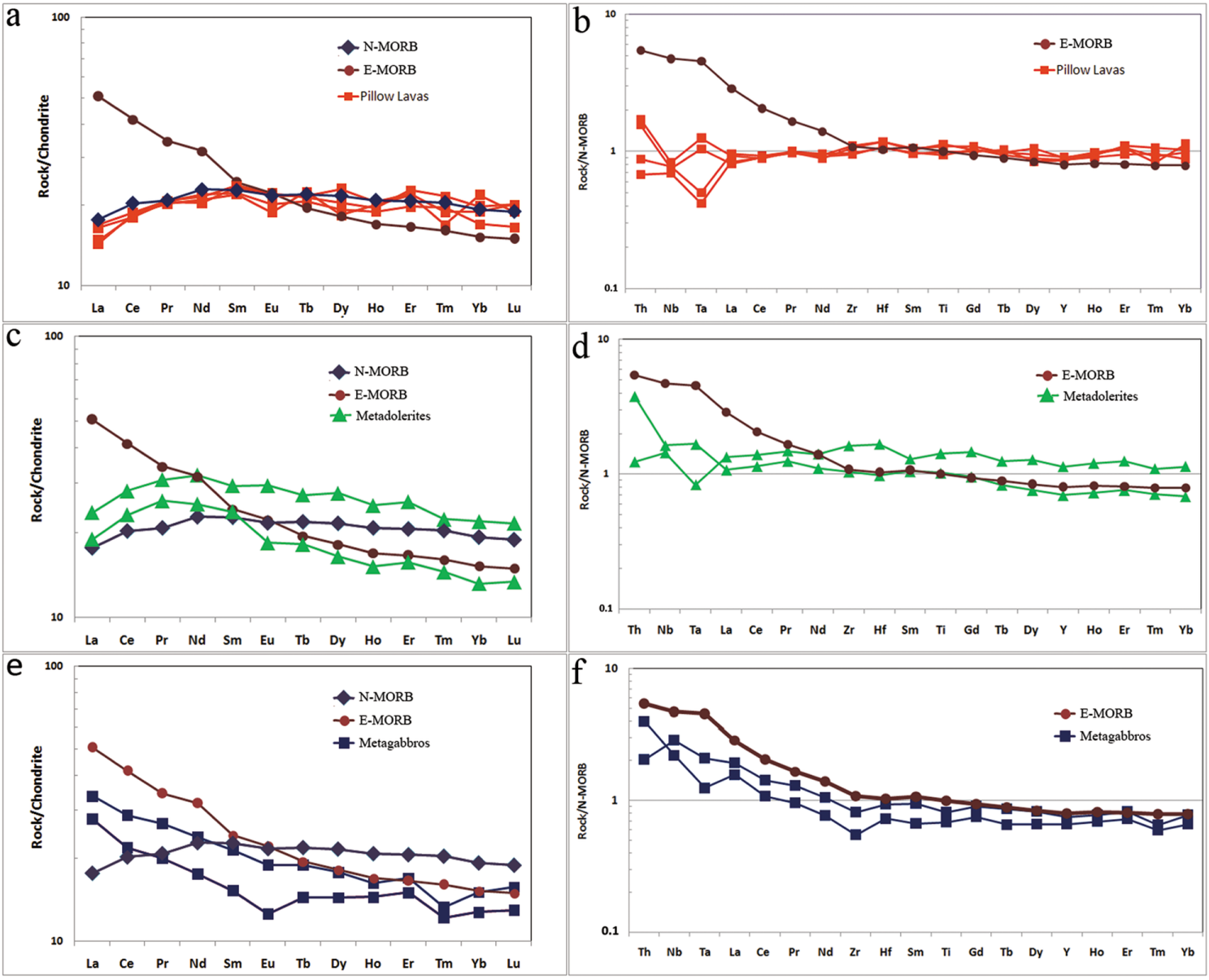
a
100
10
Rock/Chondrite
N-MORB
E-MORB
Pillow Lavas
La Ce Pr Nd Sm Eu Tb Dy Ho Er Tm Yb Lu
b
10
1
0.1
Rock/N-MORB
E-MORB
Pillow Lavas
Th Nb Ta La Ce Pr Nd Zr Hf Sm Ti Gd Tb Dy Y Ho Er Tm Yb
c
100
10
Rock/Chondrite
N-MORB
E-MORB
Metadolerites
La Ce Pr Nd Sm Eu Tb Dy Ho Er Tm Yb Lu
d
10
1
0.1
Rock/N-MORB
E-MORB
Metadolerites
Th Nb Ta La Ce Pr Nd Zr Hf Sm Ti Gd Tb Dy Y Ho Er Tm Yb
e
100
10
Rock/Chondrite
N-MORB
E-MORB
Metagabbros
La Ce Pr Nd Sm Eu Tb Dy Ho Er Tm Yb Lu
f
10
1
0.1
Rock/N-MORB
E-MORB
Metagabbros
Th Nb Ta La Ce Pr Nd Zr Hf Sm Ti Gd Tb Dy Y Ho Er Tm Yb

Figure 9

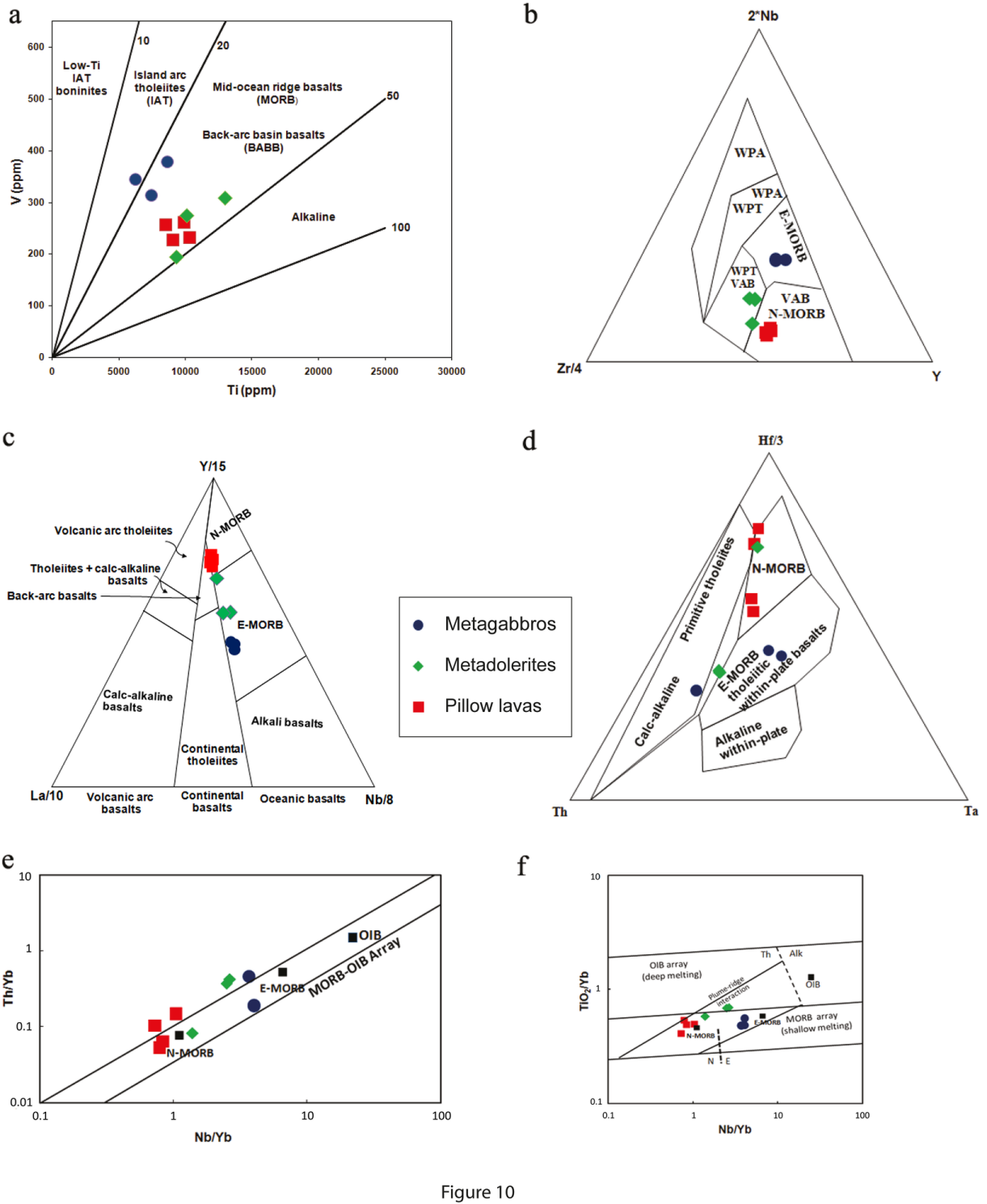
a
V (ppm)
Ti (ppm)
Low-Ti IAT boninites
Island arc tholeiites (IAT)
Mid-ocean ridge basalts (MORB)
Back-arc basin basalts (BABB)
Alkaline
10
20
50
100
b
2*Nb
Zr/4
Y
WPA
WPA
WPT
E-MORB
WPT
VAB
VAB
N-MORB
c
Y/15
La/10
Nb/8
Volcanic arc tholeiites
Tholeiites + calc-alkaline basalts
Back-arc basalts
N-MORB
E-MORB
Calc-alkaline basalts
Alkali basalts
Continental tholeiites
Volcanic arc basalts
Continental basalts
Oceanic basalts
Metagabbros
Metadolerites
Pillow lavas
d
Hf/3
Th
Ta
Primitive tholeiites
N-MORB
E-MORB tholeiitic
Within-plate basalts
Calc-alkaline
Alkaline within-plate
e
Th/Yb
Nb/Yb
OIB
E-MORB
MORB-OIB Array
N-MORB
f
TiO2/Yb
Nb/Yb
OIB array (deep melting)
Th
Alk
OIB
Plume-ridge interaction
E-MORB
N-MORB
MORB array (shallow melting)
N
E

Figure 10

SiO_2	Al_2O_3	CaO	MgO	FeO	K_2O	Na_2O	TiO_2	O	$+H_2O$
57.38	10.30	8.24	6.52	8.11	0.60	5.66	1.41	1.78	mol%

Ab: low albite; Act: actinolite; Chl: chlorite; Ep: epidote; Gln: glaucophane; Hem: hematite; Hbl: hornblende; Kfs: K-feldspar ; Ms: muscovite; Ph: phengite; Pl: plagioclase; Tnt: titanite

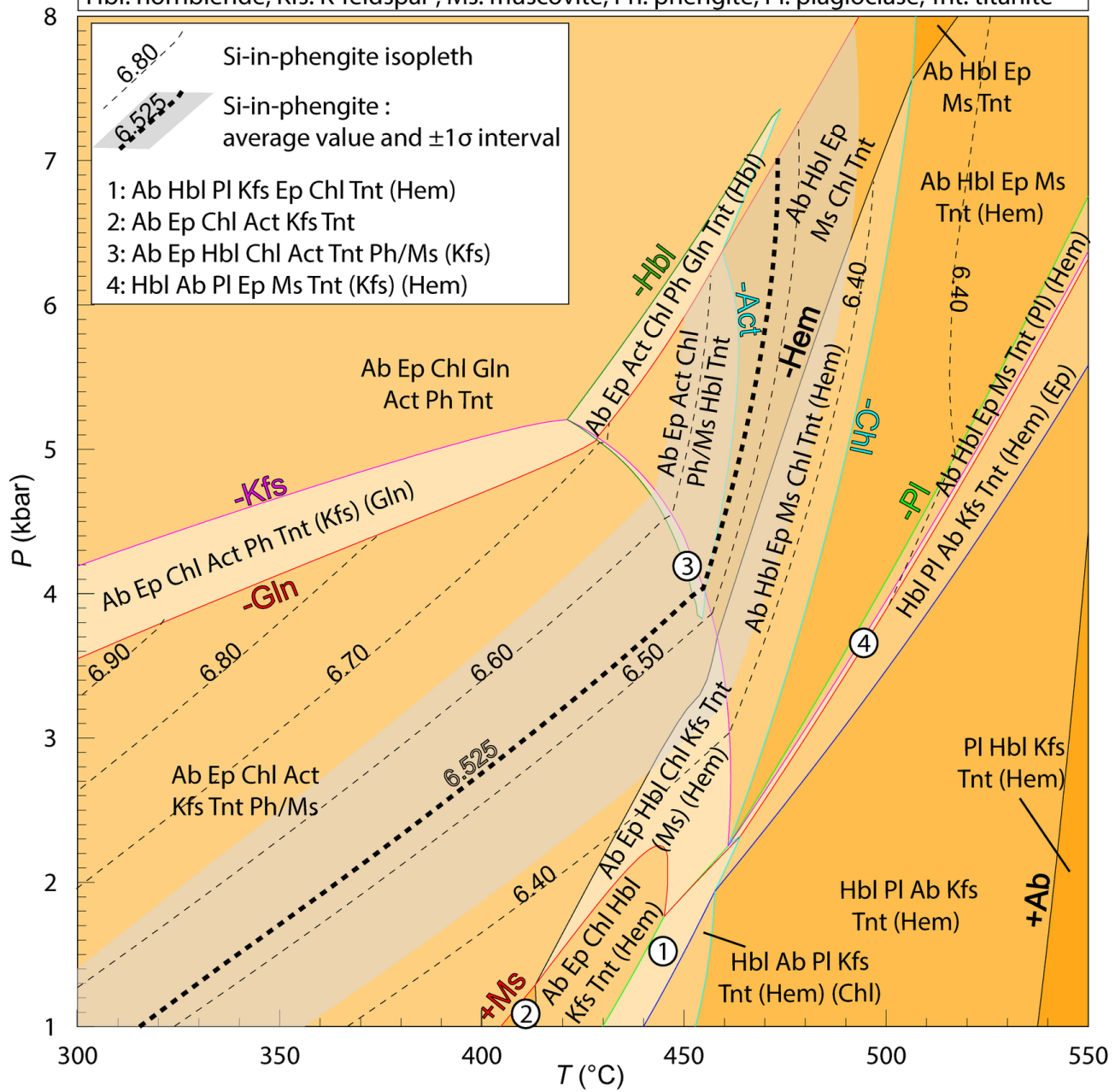

Figure 11

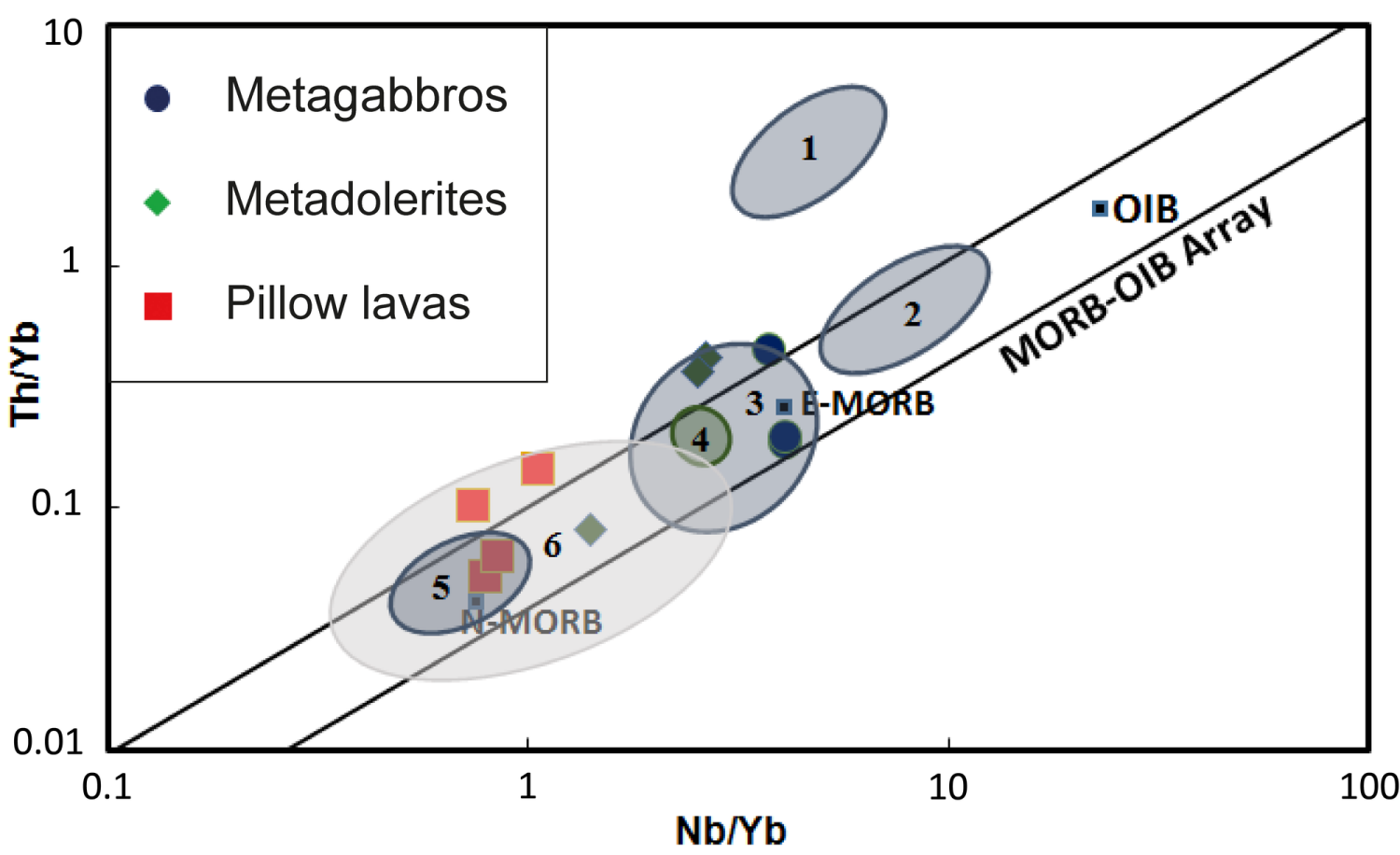
Metagabbros
Metadolerites
Pillow lavas
1
2
3
4
5
6
OIB
E-MORB
N-MORB
MORB-OIB Array
Th/Yb
Nb/Yb
10
1
0.1
0.01
0.1
1
10
100

Figure 12

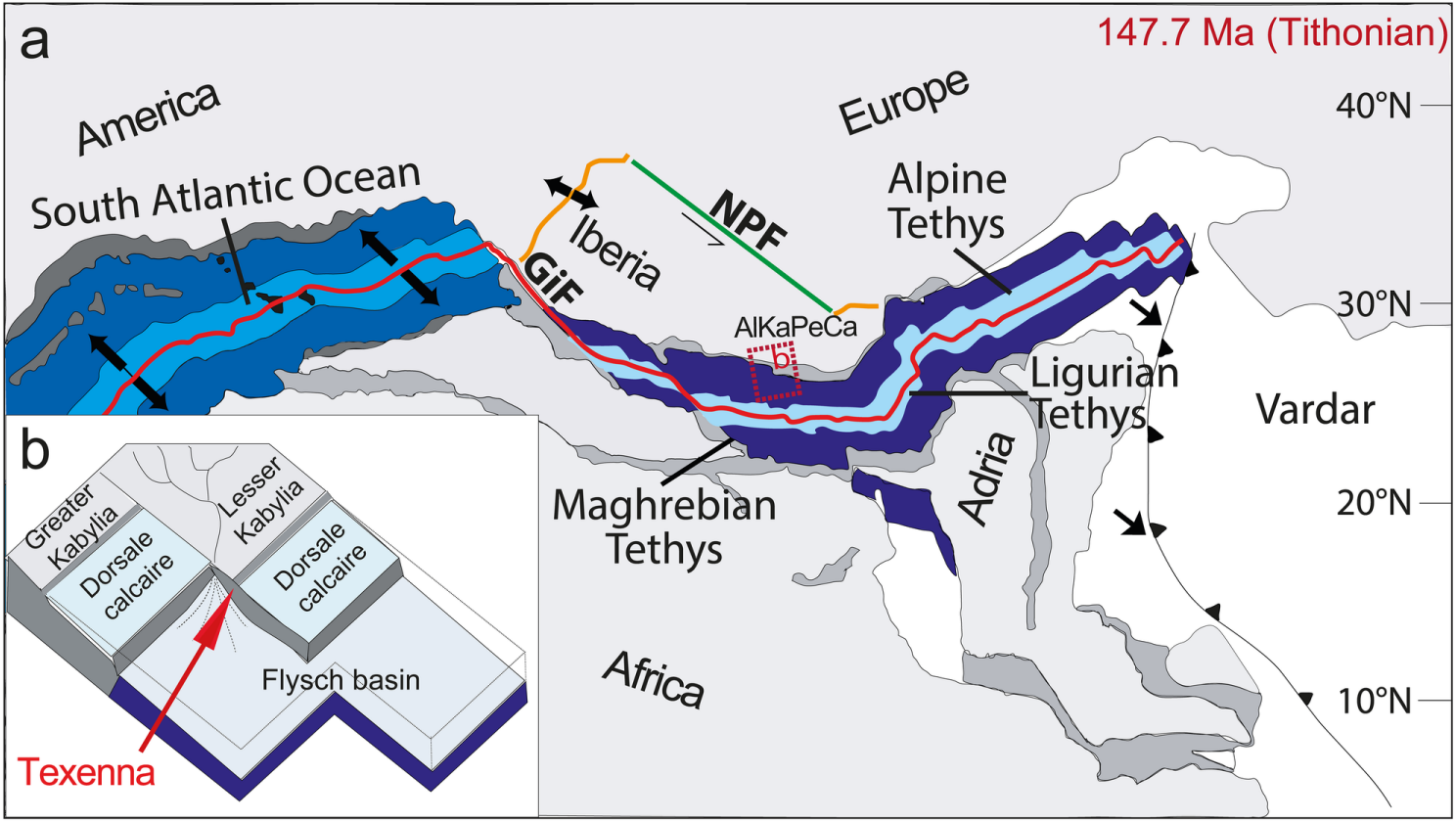
a
147.7 Ma (Tithonian)
America
South Atlantic Ocean
Europe
Iberia
GiF
NPF
Alpine
Tethys
AlKaPeCa
b
Ligurian
Tethys
Vardar
Adria
Maghrebian
Tethys
Africa
40°N
30°N
20°N
10°N
b
Greater
Kabylia
Lesser
Kabylia
Dorsale
calcaire
Dorsale
calcaire
Flysch basin
Texenna

Figure 13